An atmospheric inversion over the city of Cape Town: sensitivity analyses

Alecia Nickless[1,2], Peter J. Rayner[3], Robert J. Scholes[4], Francois Engelbrecht[5], and Birgit Erni[1,6]

[1]Department of Statistical Sciences, University of Cape Town, Cape Town, 7701, South Africa
[2]Nuffield Department of Primary Care Health Sciences, University of Oxford, Oxford, OX2 6GG, UK
[3]School of Earth Sciences, University of Melbourne, Melbourne, VIC 3010, Australia
[4]Global Change Institute, University of the Witwatersrand, Johannesburg, 2050, South Africa
[5]Climate Studies and Modelling and Environmental Health, CSIR, Pretoria, 0005, South Africa
[6]The Centre for Statistics in Ecology, the Environment and Conservation, University of Cape Town, Cape Town, 7701, South Africa

Correspondence: Alecia Nickless alecia.nickless@phc.ox.ac.uk

Abstract. We present sixteen different sensitivity tests applied to the Cape Town atmospheric Bayesian inversion analysis from March 2012 until June 2013. The reference inversion made use of a fossil fuel inventory analysis and estimates of biogenic fluxes from CABLE (Community Atmosphere Biosphere Land Exchange model). Changing the prior information product and the assumptions behind the uncertainties in the biogenic fluxes had the largest impact on the inversion results in terms

5   of the spatial distribution of the fluxes, the size of the aggregated fluxes, and the uncertainty reduction achieved. A carbon assessment product of natural carbon fluxes, used in place of CABLE, and the Open-source Data Inventory for Anthropogenic CO_2 product, in place of the fossil fuel inventory, resulted in prior estimates that were more positive on average than the reference configuration. The use of different prior flux products to inform separate inversions provided better constraint on the posterior fluxes compared with a single inversion. For the Cape Town inversion we showed that, where our reference

10   inversion had aggregated prior flux estimates that were made more positive by the inversion, suggesting that the CABLE was overestimating the amount of CO_2 uptake by the biota, when the alternative prior information was used, fluxes were made more negative by the inversion. As the posterior estimates were tending towards the same point, we could deduce that the best estimate was located somewhere between these two posterior fluxes. We could therefore restrict the best posterior flux estimate to be bounded between the solutions of these separate inversions.

15   The assumed error correlation length for NEE fluxes played a major role in the spatial distribution of the posterior fluxes and in the size of the aggregated flux estimates, where ignoring these correlations led to posterior estimates more similar to the priors compared with the reference inversion. Apart from changing the prior flux products, making changes to the error correlation length in the NEE fluxes resulted in the greatest contribution to variability in the aggregated flux estimates between different inversions. Those cases where the prior information or NEE error correlations were altered resulted in greater

20   variability between the aggregated fluxes of different inversions compared with the uncertainty around the posterior fluxes of the reference inversion.

Solving for four separate weekly inversions resulted in similar estimates for the weekly fluxes compared with the single monthly inversion, while reducing computation time by up to 75 %. Solving for a mean weekly flux within a monthly inversion did result in differences in the aggregated fluxes compared with the reference inversion, but these differences were mainly during periods with data gaps. The uncertainty reduction from this inversion was almost double that of the reference inversion

5 (47.2% versus 25.6%). Taking advantage of more observations to solve for one flux, such as allowing the inversion to solve for separate slow and fast components of the fossil fuel and NEE fluxes, as well as taking advantage of expected error correlation between fluxes of homogeneous biota, would reduce the uncertainty around the posterior fluxes. The sensitivity tests demonstrate that going one step further and assigning a probability distribution to these parameters, for example in a hierarchical Bayes approach, would lead to more useful estimates of the posterior fluxes and their uncertainties.

10 *Copyright statement.*

1   Introduction

Atmospheric inversion, where estimates of CO_2 fluxes can be derived from measurements of CO_2 concentrations at a point location, is a useful tool for monitoring, reporting and verification (MRV) of CO_2 emissions from cities (Bellassen and Stephan, 2015; Wu et al., 2016; Lauvaux et al., 2016; Oda et al., 2017a). Estimates of city-level CO_2 emissions are usually obtained

15 using bottom-up techniques, which require some knowledge of what activities produce CO_2 emissions and the fuel usage of these activities. Ascertaining the uncertainty in these inventory-based estimates is not trivial, and these uncertainties increase as the spatio-temporal resolution of these estimates is increased (Turnbull et al., 2011). The inversion solves for both the anthropogenic and biogenic contributions, usually expressed as fluxes of CO_2. This approach attempts to correct prior estimates of these fluxes such that the misfit between the observed and modelled concentrations at the measurement sites is minimised.

20 Therefore, if an inventory analysis of fossil fuel emissions from the city is used as the prior information, the inversion will provide corrections to these emissions.

Inversions used for investigating city-level emissions are carried out at kilometric resolutions (Bréon et al., 2015; Lauvaux et al., 2016). Such an inversion was carried out for the city of Cape Town, South Africa (Nickless et al., 2018). As is required for all atmospheric inversions, decisions need to be made regarding what prior information should be used; for which unknown

25 CO_2 fluxes will the inversion solve; and what the structure of the covariance matrices will be (Bréon et al., 2015; Lauvaux et al., 2016; Staufer et al., 2016; Oda et al., 2017a). Sensitivity tests on the impact of these decisions are necessary, and provide information on the robustness of the inversion results. This paper presents the results of sensitivity tests applied to these decisions for the Cape Town inversion.

The prior information required for an atmospheric inversion are the initial estimates of the unknown fluxes. For a city-level

30 inversion, this means initial estimates of the gridded fossil fuel emissions, at the spatio-temporal scale at which the inversion is to be performed. The inversion described in Nickless et al. (2018) made use of a bespoke inventory analysis carried out

for the purpose of the inversion (Nickless et al., 2015a). Information on the uncertainty in these prior fluxes is also required. The uncertainties applied to the estimates of the fossil fuel fluxes for Cape Town were based on error propagation techniques. The uncertainties in the emission factors and activity data were combined to obtain an overall uncertainty in the flux estimate (Nickless et al., 2015a).

5   The observed concentration data, as measured at atmospheric monitoring sites and which are the data used by an atmospheric inversion, are as a result of aggregated fluxes from all sources of CO_2 along the path of the air flow. Sources refer to anything which may have a positive (i.e. emit) or negative (i.e. uptake) contribution to the overall CO_2 concentration. Even if biogenic fluxes are not necessarily of interest in the city-level inversion, they need to be accounted for in the model as these fluxes will be inducing changes to the observed CO_2 concentration. For the Cape Town inversion, net ecosystem exchange (NEE) fluxes were

10 obtained from the land atmosphere exchange model CABLE (Community Atmosphere Biosphere Land Exchange) (Nickless et al., 2018). This model was dynamically coupled to the regional climate model, CCAM (Conformal Cubic Atmospheric Model), from which climatic variables, required for the atmospheric transport model, were obtained. Uncertainties in the prior fluxes were specified to be large due to the large amount of variation in modelling ecosystem productivity and respiration from the fynbos biome by dynamic vegetation models (Moncrieff et al., 2015). Fynbos is the dominant naturally occurring vegetation

15 type in the area. Cape Town city is also surrounded by large agricultural areas, particularly vineyards. The uncertainties in the prior NEE fluxes were set at the estimate of net primary productivity (NPP). NEE = NPP + Rh, where Rh is the heterotrophic respiration. Therefore NEE is a balance of two large fluxes, which are both non-trivial to model (Archibald et al., 2009). The uncertainty in set as the productivity component of the NEE flux as the error in the estimate of NEE can be as large as either the productivity or respiration component. Therefore, for the Cape Town inversion, the uncertainty was much larger than the

20 accompanying NEE estimate. We emphasize these details, as the sensitivty analyses will demonstrate the importance of the approach adopted for assigning uncertainties and error correlations to these natural fluxes.

    Using the inversion described in Nickless et al. (2018) as the reference inversion, we carried out sensitivity analyses which considered alternative products for the prior information. For the prior fossil fuel fluxes, we substituted the estimates from the bespoke inventory analysis with those from the ODIAC (Open-source Data Inventory for Anthropogenic CO_2) product (Oda

25 and Maksyutov, 2011; Lauvaux et al., 2016; Oda et al., 2017a; Oda et al. , 2017b). For the biogenic fluxes, we performed a test where the CABLE estimates were replaced with those from a carbon assessment study (Scholes et al., 2013). The carbon assessment study aimed to map terrestrial carbon stocks for South Africa and provided estimates of NPP and NEE at a spatial resolution of $1\,km \times 1\,km$, and was used for a previous optimal measurement network design study for South Africa (Nickless et al., 2015b). Sensitivity tests were performed where the original products were used for the prior fossil fuel and NEE fluxes,

30 but the uncertainties prescribed to these fluxes were either individually doubled or halved, which therefore changed the relative contribution of each flux to the uncertainty in the total prior flux.

    The structure of the uncertainty covariance matrices for the observations and for the prior fluxes can have a significant effect on the resulting flux estimates from the inversion, as well as on the spatial distribution of these fluxes (Lauvaux et al., 2016). We investigated the impact of the prescribed off-diagonal covariances in these prior covariance matrices. In the reference inver-

35 sion we allowed a small correlation length of one hour between observation errors. For the prior NEE uncertainty estimates, a

correlation length of one kilometre was specified for NEE fluxes from the same week. No spatial correlation was specified between fossil fuel flux uncertainties as many of the larger sources from the inventory analysis were point sources. As we did not solve for fossil fuel fluxes from different sectors separately, we decided it would be better to keep fossil fuel flux uncertainties uncorrelated. This would avoid implausible correlations between uncertainties; for example, between a large industrial source

5 and a residential source. As sensitivity tests, we removed each of these correlations from the prescribed uncertainty covariance matrices; individually as well as the case where the uncertainty covariance matrices for both the observations and for the prior fluxes were specified as diagonal matrices.

We were interested in the composition of the control vector, which contains the unknown surface fluxes and domain boundary concentrations. For the reference inversion we carried out thirteen monthly inversions which solved for weekly fluxes from

10 each of the 101×101 surface pixels. The weekly fluxes consisted of working week and weekend fossil fuel fluxes, and NEE fluxes for the full week; each separated into day and night fluxes. Each monthly inversion solved for four sets (i.e. a period of four weeks) of these six distinct weekly fluxes from each pixel. We tested whether solving for an average of each of these weekly fluxes over the course of the month would achieve similar results compared with the reference inversion. We also compared the reference inversion with the approach of carrying out separate inversions for each week. Therefore instead of

15 performing 13 monthly inversions, we performed 13×4 weekly inversions; four inversions per month. Each of these cases requires considerably less computational resources to perform an individual inversion. If either of these alternative control vectors provides sufficiently similar results to the reference case, this would provide a more efficient means of conducting the inversion. This would allow more alternative configurations of other components of the inversion framework to be tested in the same period of time.

20 The Cape Town inversion differs from recent city-scale inversions carried out over mega cities (Bréon et al., 2015; Staufer et al., 2016) due to the high integration of natural areas in the city borders of Cape Town. Natural fluxes are an important contributor to the CO_2 budget of the region. For example, Table Mountain National Park is located directly adjacent to the city bowl. In fact the city wraps around the base of the mountain. This national park covers an area of $221 \, \text{km}^2$. For this reason, the gradient method, which relies on the difference between pairs of measurement sites when the wind is blowing from one site,

25 over the target region, to the second site, would not be appropriate given locations of our two measurement sites. In our case, if the air travelled between the two sites, it would pass directly over Table Mountain National Park, and therefore the gradient method would not have the desired effect of diminishing the impact of biogenic fluxes along the transect between the two sites. In addition, the wind fields showed that air did not travel in a straight path between our two sites (Nickless et al., 2018).

We adopted the approach usually used from regional inversions, where the inversion modelled the concentrations at the

30 measurement sites (Lauvaux et al., 2012). Instead of subtracting the background CO_2 concentration from the measurements, which would have arrived from one of the domain boundaries, we solved for the concentrations at the boundary and therefore included these in the control vector, similar to the approach of Lauvaux et al. (2016). We kept tight constraints on what these concentrations could be, and used the background measurements obtained from Cape Point as prior estimates of these concentrations. We were able to do this as there are no large anthropogenic sources near the boundary of the domain. We

showed in the reference inversion that the variation in the total CO_2 was largely driven by the variation in the NEE flux. In these sensitivity analyses we investigate the impact of reduced uncertainty assigned to the prior NEE estimates.

The purpose of this paper is to present the results of these sensitivity tests in comparison with the Cape Town reference inversion. Based on these tests, conclusions can be drawn on how well the reference inversion was specified, and which

5 components could be improved with highest priority to give the greatest improvement in the estimation of the posterior fluxes. Section 2 briefly introduces the Bayesian inversion framework. Details of the reference inversion can be found in Nickless et al. (2018). This is followed by a description of the alternative prior information products. The details of the sensitivity analysis are provided. The results of the sensitivity analyses are provided in section 3, followed by discussion of these results in section 4, and conclusions in section 5.

2 Methods

Characterisations of the two observational sites installed at Robben Island and Hangklip lighthouses, and the background monitoring site at Cape Point, are provided in (Nickless et al., 2018). Measurements of CO_2 concentrations were obtained between March 2012 and June 2013 by means of a Picarro Cavity Ring-down Spectroscopy (CRDS) (Picarro G2301) instrument. Sufficient data for 13 of the 16 months were available to perform monthly inversions. Robben Island site viewed predominantly

15 air influenced by the Cape Town city bowl whereas Hangklip viewed air influenced by biogenic fluxes from nearby fynbos vegetation and agricultural areas.

In the next section we describe the Bayesian inverse modelling framework and the details of the reference Cape Town inversion (referred to in short-hand as inversion **Ref**). In sections 2.3 to 2.6 we describe the alterations we considered to the reference inversion, and how we compared the results between different inversions.

2.1 Bayesian inverse modelling framework and the reference inversion

Nickless et al. (2018) used the Bayesian inverse modelling framework to model CO_2 hourly concentrations at Robben Island and Hangklip measurement sites. This approach solves for the unknown sources, as defined in the control vector, s, using the Bayesian least squares solution as described in Tarantola (2005),

25 $$s = s_0 + \mathbf{C}_{s_0}\mathbf{H}^T\left(\mathbf{H}\mathbf{C}_{s_0}\mathbf{H}^T + \mathbf{C}_c\right)^{-1}(c - \mathbf{H}s_0) \qquad (1)$$

and the solution for the posterior error covariance matrix for the sources, $\mathbf{C}_s$,

$$\mathbf{C}_s = \left(\mathbf{H}^T\mathbf{C}_c^{-1}\mathbf{H} + \mathbf{C}_{s_0}^{-1}\right)^{-1} \qquad (2)$$

30 $$= \mathbf{C}_{s_0} - \mathbf{C}_{s_0}\mathbf{H}^T\left(\mathbf{H}\mathbf{C}_{s_0}\mathbf{H}^T + \mathbf{C}_c\right)^{-1}\mathbf{H}\mathbf{C}_{s_0} \qquad (3)$$

where c is the vector of CO_2 concentration measurements from Robben Island and Hangklip measurement sites, s_0 is the vector of prior estimates of these sources, $\mathbf{C}_c$ the error covariance matrix of c, and $\mathbf{C}_{s_0}$ the prior uncertainty covariance matrix of s_0. $\mathbf{H}$ is the Jacobian matrix representing the first derivative of the modelled concentration, c_{mod}, at the observational site and dated with respect to the elements of s. $\mathbf{H}$ projects the elements of s into the observation space of c:

$$c_{mod} = \mathbf{H}s. \tag{4}$$

The sources, s, consisted of gridded surface fluxes contained within the domain and concentrations of CO_2 at the boundary. The spatial resolution of inversion was set at $1\,\mathrm{km}$ by $1\,\mathrm{km}$ and the extent of the domain was between $34.5°$ and $33.5°$ south and between $18.2°$ and $19.2°$ east.

Separate monthly inversions were performed. s contained six surface fluxes from each of the $101{\times}101$ surface pixels for each of the four weeks. The surface fluxes included working week and weekend fossil fuel fluxes and weekly NEE fluxes, each separated into day and night fluxes. Therefore a monthly inversion solves for $10{,}201{\times}6{\times}4 = 244{,}824$ surface fluxes. The boundaries were considered as the edge of the domain at each cardinal direction (north, east, south, and west). The boundary concentrations in s consisted of four average weekly concentrations at the four boundaries, separated into day and night averages, therefore 32 boundary concentrations.

The observed CO_2 concentrations, c, consisted of hourly averaged concentrations derived from the instantaneous measurements obtained at Robben Island and Hangklip. As the parameters of the atmospheric transport model are not constrained by the inversion, the resulting errors in the modelled concentrations can be added to the measurement errors contained in $\mathbf{C}_c$ (Tarantola, 2005). The diagonal elements of the observation error covariance matrix, $\mathbf{C}_c$, consisted of daytime error variances of $4\,\mathrm{ppm}^2$ and night-time errors of $16\,\mathrm{ppm}^2$. Night-time errors in modelled concentrations are set higher at night than during the day as the planetary boundary layer (PBL) is lower at night (Feng et al., 2016; Lauvaux et al., 2016). The PBL is characterised by continuous turbulence, whereas turbulence is lacking above this layer, and its height changes in response to thermal stratification. It has significant impact on weather, climate, and the hydrologic cycle (Zhang et al., 2014). These error variances accounted for measurement errors, atmospheric transport modelling errors, representation errors and aggregation errors. As described in Nickless et al. (2018), to account for meteorological conditions, these error variances were inflated by up to $1\,\mathrm{ppm}^2$ during day and $4\,\mathrm{ppm}^2$ at night depending on the wind speed, with still conditions leading to the maximum error inflation. An additional inflation factor was added equal to the observed variance of the instantaneous CO_2 concentration measurements made within the hour. These additional inflations represented periods when the atmospheric transport model would have been most likely to misrepresent the atmospheric transport.

The off-diagonal elements of $\mathbf{C}_c$ were calculated, based on the Balgovind correlation model as used in Wu et al. (2013), as:

$$C_c(c_i, c_j) = \sqrt{C_c(c_i)}\sqrt{C_c(c_j)}(1 + \frac{h}{L})exp(-\frac{h}{L}) \tag{5}$$

where c_i and c_j are the average concentrations during hours i and j, $C_c(c_i)$ and $C_c(c_j)$ the corresponding error variances for the concentrations in hours i and j, the characteristic correlation length L was assumed to be 1 hour, and h is the length in time between observations i and j. The impact of this, albeit short, correlation length was assessed in a sensitivity test where no

5   correlation between the observation errors was assumed. No consensus has yet been reached on how these correlations between model errors in the concentrations should be treated (Lauvaux et al., 2016).

We used the regional climate model CCAM, run in variable-resolution mode with Cape Town at its centre and driven by NCEP (National Centres for Environmental Prediction) reanalysis data, to produce three-dimensional fields of mean winds (u, v, w), potential temperature and turbulent kinetic energy (TKE) (McGregor and Dix, 2001; Roux, 2009; Engelbrecht et al.,

10   2013). The model produced hourly estimates on a $1\,\mathrm{km} \times 1\,\mathrm{km}$ spatial grid, which extended from between $34.5°$ and $33.5°$ south and between $18.2°$ and $19.2°$ east. These variables were used to drive a Lagrangian particle dispersion model (LPDM) (Uliasz, 1994). LPDM simulates atmospheric transport by releasing particles from the observational sites and tracking these particles backward in time. These particle counts can be used to derive the elements of the Jacobian matrix $\mathbf{H}$ as originally described by Seibert and Frank (2004) and subsequently used in several inversion studies (Lauvaux et al., 2012; Wu et al.,

15   2013; Ziehn et al., 2014; Nickless et al., 2015b; Lauvaux et al., 2016; Nickless et al., 2018; Oda et al., 2017a). The details of this as pertaining to the Cape Town reference inversion are described in Nickless et al. (2018). The number of rows in $\mathbf{H}$ are equal to the number of hourly concentrations assimilated into the inversion and the number of columns is equal to the number of sources solved for in the control vector, $\boldsymbol{s}$.

The prior fossil fuel fluxes were estimated from a bespoke inventory analysis carried out for Cape Town. Details are provided

20   in Nickless et al. (2015a) and Nickless et al. (2018). The inventory analysis includes fossil fuel emissions from industrial point sources, road vehicle transport emissions, airport and harbour emissions, and residential emissions. Residential emissions were based on the assumed use of raw fossil fuels for heating, lighting and cooking. The largest point source was a crude oil refinery located north east of the central business district (CBD).

Uncertainties in these fossil fuel estimates were derived based on error propagation techniques (Nickless et al., 2015a). In

25   the next section we present a comparison between the uncertainties assigned in the reference inversion with those assigned to the inversion using the ODIAC fossil fuel fluxes (see Figure 2). The largest uncertainties, as a percentage of the fossil fuel flux estimate, were for those associated with residential emissions, which were spatially distributed according to the 2011 population census. These uncertainties were set at 60% of the domestic emissions estimate. Point sources had relatively smaller uncertainties, as these estimates were based on reported fuel usage data, which was assumed to be accurate, but in absolute

30   terms these uncertainties were large contributors to the total fossil fuel flux uncertainty. Fossil fuel emissions from all sources were summed to provide a total fossil fuel flux for the working week and weekend, separately for day and night. No correlation was assumed between uncertainties in the fossil fuel sources. This was to avoid creating unlikely correlations between fluxes from different sources. We assumed no correlation in time between fossil fuel fluxes as we were already solving for weekly averaged fluxes, which effectively assumes 100% correlation between fluxes in the same week.

Prior estimates of the NEE fluxes were obtained from the land atmosphere exchange model CABLE (Kowalczyk et al., 2006). The model produced hourly estimates of NEE, which were aggregated into weekly (day and night) flux estimates in units of $kg\,CO_2\,m^{-2}\,week^{-1}$, and used as the prior estimates of terrestrial biogenic fluxes. The spatial resolution of these prior NEE fluxes were kept at a $1\,km \times 1\,km$ resolution. We selected CABLE to produce our NEE estimates as CCAM had been

5   dynamically coupled to this land surface model, which allowed for feedbacks between land surface and climate processes, such as leaf area feedback on maximal canopy conductance and latent heat fluxes (Zhang et al., 2013).

The CO_2 fluxes over the ocean were obtained from a study that characterised the seasonal cycle of air-sea fluxes of CO_2 in the southern Benguela upwelling system off the South African west coast (Gregor and Monteiro, 2013). Daily CO_2 fluxes were derived from measurements of pCO_2. These daily fluxes were used to derive weekly flux estimates, which were averaged

10   over a monthly period, and applied as prior estimates to the ocean surface grids within the domain.

As the fynbos biome, which covers a large proportion of the terrestrial surface in our domain, is poorly represented by dynamic vegetation models (Moncrieff et al., 2015), the uncertainties assigned to the NEE estimates were large. Previous studies, for example, have shown that the model forms used for the soil temperature-respiration function and the soil moisture-respiration function have large impacts on the NEE estimates, with resulting NEE estimates differing by over 100% compared

15   with eddy-covariance measurements (Exbrayat et al., 2013). We assigned the value of the NPP associated with the terrestrial NEE estimate as the uncertainty value. For the ocean fluxes, the standard deviations in the daily CO_2 fluxes from Gregor and Monteiro (2013) were assigned as the uncertainties. As the uncertainties in NEE estimates were likely to be related, spatial error correlations between NEE fluxes were incorporated in the off-diagonal elements of $\mathbf{C}_{s_0}$. The off-diagonal elements were calculated in an analogous manner to those for $\mathbf{C}_c$, where $C_{s_{0;NEE}}(s_{NEE;i})$ and $C_{s_{0;NEE}}(s_{NEE;j})$ were the corresponding

20   variances in the NEE flux uncertainty matrix for pixels i and j, the characteristic correlation length L was assumed to be $1\,km$, and h was the spatial distance between pixels i and j. Non-zero error covariances were allowed between NEE estimates from the same week. We assumed no error correlation between fossil fuel and NEE fluxes.

Sections 2.2 to 2.5 describe alterations made to the reference inversion for the purpose of sensitivity analyses.

2.2   Alternative biogenic flux product

25   As part of a project which aimed to assess the carbon sinks of South Africa (DEA, 2015), a report together with monthly $1\,km \times 1\,km$ estimates of terrestrial carbon stocks and fluxes were produced (Scholes et al., 2013). To estimate these fluxes, a distinction was made between carbon stocks in natural to semi-natural areas and those on transformed land, such as annually-cropped cultivated land, plantation forests, and urban areas (which was based on the IPCC 2006 value for closed urban forests). We used these estimates of NEE and NPP in place of those from CABLE (inversion **Carbon Assess**).

30   To estimate gross primary productivity (GPP), ten years (2001 to 2010) of monthly climatologies (temperature, rainfall, relative humidity) and satellite products for photosynthetically active radiation (PAR) and fraction of absorbed photosynthetically active radiation (FAPAR) were assimilated. Autotrophic respiration (Ra) was calculated based on the inputs for temperature, above-ground biomass, below-ground biomass and FAPAR. NPP could then be calculated as NPP = GPP - Ra. The hetrotrophic component (Rh) of Ecosystem respiration (Re) was based on estimates of soil organic carbon stocks and above-ground litter.

The basic calculation to obtain NEE was NEE = GPP - Re, and additional losses of CO_2 through biomass burning, and export and import fluxes from harvest and trade-related activities were accounted for.

To disaggregate the monthly products into day and night fluxes, it was assumed that all GPP took place during the day, and that half of Re occurred during the day and half at night. Therefore the weekly NEE and NPP estimates used for the prior
5   information in the inversion were based on the GPP and respiration products from the assessment. The GPP flux for the year in the fynbos biome was estimated to be $521\,\mathrm{g}\ CO_2\ \mathrm{m}^{-1}\mathrm{year}^{-1}$ with a standard deviation of $492\,\mathrm{g}\ CO_2\ \mathrm{m}^{-1}\mathrm{year}^{-1}$. Therefore, as for the CABLE estimates used in the reference inversion, we assign uncertainties to the prior NEE estimates equal to the NPP estimate. A map of the prior daytime NEE fluxes in May 2012 from the CABLE and carbon assessment products is provided in Figure 1.
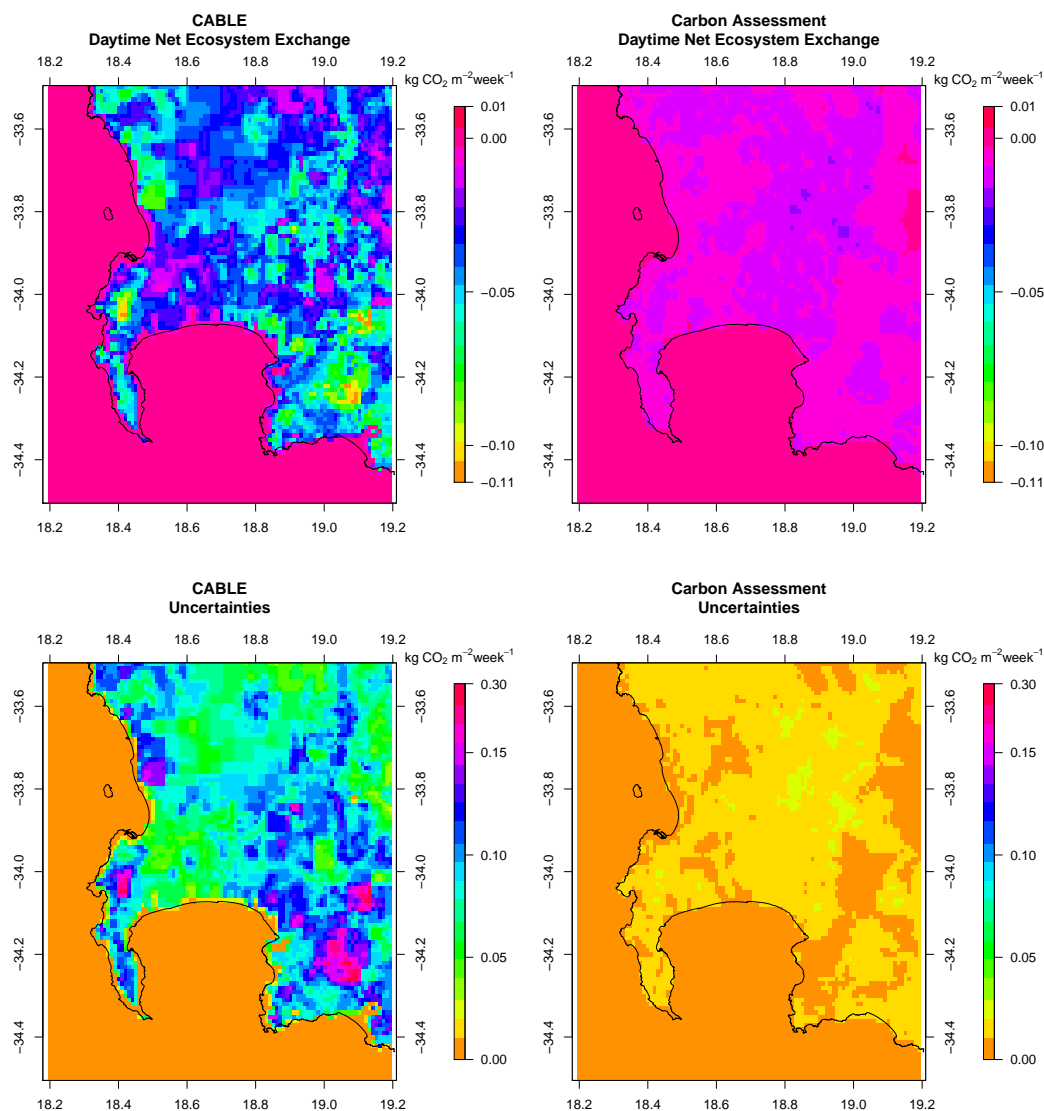
Figure 1. Spatial distribution of the prior daytime NEE fluxes produced by CABLE (top left) and the carbon assessment product (top right) in May 2012, as well as the uncertainty estimates assigned to these fluxes (bottom row).

2.3 Alternative fossil fuel emissions product

As an alternative to the inventory analysis of the fossil fuel fluxes, we used current estimates of anthropogenic fossil fuel emissions from the $1\,\text{km} \times 1\,\text{km}$ ODIAC product for the years 2012 and 2013 (ODIAC2017) (Oda and Maksyutov, 2011; Lauvaux et al., 2016; Oda et al., 2017a; Oda et al. , 2017b) (inversion **ODIAC**). The product provides monthly emissions

5 of CO_2 in kt of carbon. The original ODIAC product (Oda and Maksyutov, 2011) made use of global energy consumption statistics and distributed the emissions from these activities based on known point source emitters, such as power plants, and on a global nightlight distribution satellite product. Emissions from point sources, such as those from power plants, were estimated separately from the diffuse emissions, for example those due to transport. These emissions were disaggregated onto to a $1\,\text{km} \times 1\,\text{km}$ grid. The updated product has further disaggregated the diffuse emissions to a $30\,\text{m} \times 30\,\text{m}$ grid by making use of global

10 road network data, a satellite product on surface imperviousness, and population census data (Oda et al., 2017a; Oda et al. , 2017b). This $30\,\text{m} \times 30\,\text{m}$ diffuse emission product together with the point source emission product were aggregated back up to the $1\,\text{km} \times 1\,\text{km}$ grid. An inversion carried out for Indianapolis, IN, making use of the updated ODIAC product has shown it to produce similar corrections to the fluxes as those from the inversion making use of the Hestia inventory product (Oda et al., 2017a). The Hestia product is a fine-grained - down to the street/building level - bottom-up CO_2 emission product which makes

15 use of information from building energy simulation models, traffic data, power production reporting, and pollution reporting (Gurney et al., 2012). This product is available for a few cities in the United States, including Indianapolis.

The monthly estimates were re-scaled according to the day of the week and to the hour of day using scaling factors for South Africa as estimated by Nassar et al. (2013). These estimates were re-aggregated into day and night working week and weekend fossil fuel fluxes in units of $\text{kg}\,CO_2\,\text{m}^{-2}\,\text{week}^{-1}$. These estimates for the fossil fuel fluxes were used as prior estimates for the

20 inversion in place of the inventory-based estimates used for the reference inversion. The daytime fossil fuel fluxes produced by the inventory analysis and the ODIAC product are provided in Figure 2.
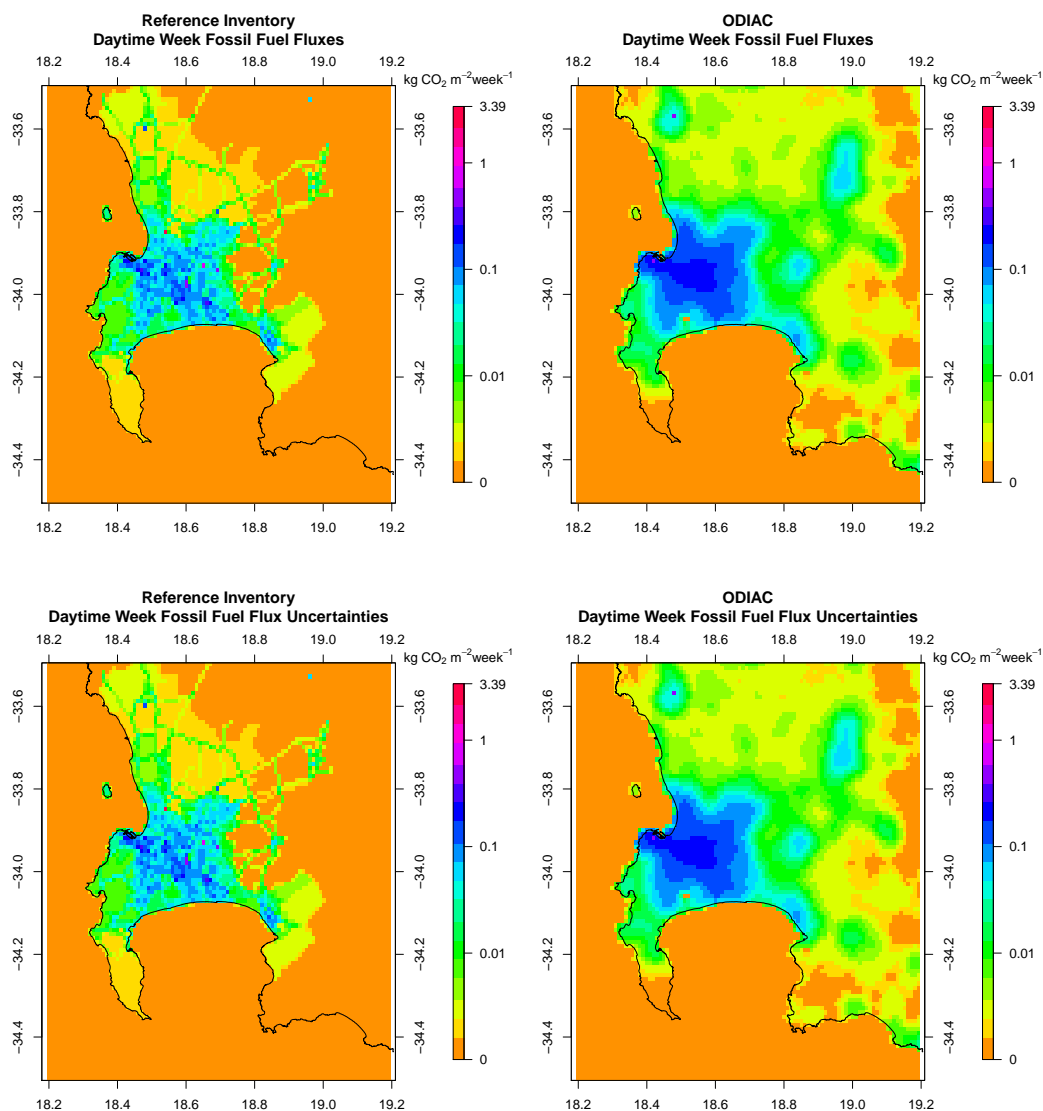
Figure 2. Spatial distribution of the prior fossil fuel fluxes produced from the Cape Town inventory analysis (top left) and the ODIAC fossil fuel product (top right) in May 2012, as well as the uncertainty estimates assigned to these fluxes (bottom row).

2.4 Alternative covariance structures

The specification of the prior uncertainty covariance structures have been shown to have a significant impact on the pixel-level flux estimates, the total flux estimate for the domain, and on the spatial distribution of the fluxes (Wu et al., 2013; Lauvaux et al., 2016). For example, in the Indianapolis inversion, assuming correlation lengths of 4 or 12 km in the prior uncertainty

5 covariance matrix of the fluxes resulted in total flux estimates for the city that were 17 and 25% larger than the total flux estimate assuming no correlation (Lauvaux et al., 2016). The effect of changing the correlation length had a larger impact on the total flux estimate than changing the prior emission product from Hestia to ODIAC.

To assess the sensitivity of the posterior flux estimates, their uncertainties, and their distribution in space to the specification of the covariance matrix, we considered inversions where the non-zero off-diagonal elements of $\mathbf{C}_{s_0}$ and $\mathbf{C}_c$ were set to zero.

10 We considered an inversion which assumed no temporal error correlation in the specification of $\mathbf{C}_c$ (inversion **NEE Corr**), an inversion where no spatial error correlation was assumed for $\mathbf{C}_{s_0}$ (inversion **Obs Corr**), and an inversion which assumed no error correlations in the specification of $\mathbf{C}_{s_0}$ and $\mathbf{C}_c$ (inversion **No Corr**).

We also considered inversions where the prior fossil fuel flux uncertainty was doubled (inversion **Double FF**) and where it was halved (inversion **Half FF**), and similarly for the NEE flux uncertainties (inversions **Double NEE** and **Half NEE**). By

15 doubling or halving the uncertainty of the fossil fuel or NEE component of the total flux, we changed the relative uncertainty contribution of each of these had to the total uncertainty when compared with the reference inversion.

Due to the large impact that the estimation of the domestic fossil fuel emissions had on the temporal profile of the total fossil fuel fluxes, we considered a modification of the estimated domestic emissions in the inventory product. In the reference inversion 75% of the domestic emissions from heating were assumed to take place during the six winter months. We tested

20 the impact of this assumption by altering the domestic emissions so that they were distributed uniformly through time, but still spatially distributed according to the population size. This changes the prior estimates of the fossil fuel fluxes and their distribution through time, as well as their uncertainties, which were set at 60% of the domestic emission estimate (inversion **Domestic Homogenised**).

Due to the large uncertainty in the modelling of NEE (Zhang et al., 2013; Moncrieff et al., 2015), particularly over the fynbos

25 biome, we considered that perhaps the average of the NEE estimates from CABLE over the domain may be a more reliable representation of the true flux compared with the pixel-level estimates. Therefore we averaged the NEE and NPP estimates from CABLE over the inversion domain and assigned this average NEE, and NPP for its uncertainty, as the prior biogenic flux estimates (inversion **NEE Homogenised**).

We considered an inversion where the uncertainties in $\mathbf{C}_c$ were set at 2 ppm for the day and 4 ppm at night (inversion **Simp**

30 **Obs Error**). In this case all the errors in the modelled concentrations are contained within these values, and we disregard the climatic conditions under which the measurements were taken. We tested the impact of increasing the night-time uncertainty in the observation errors to 10 ppm (inversion **Simp Obs with Large Night**). We further simplified $\mathbf{C}_c$ by performing an inversion which disregarded the temporal correlation which was assumed for the reference inversion (inversion **Simp Obs No Corr**).

2.5 Alternative control vectors

In the reference inversion the total CO_2 flux from a single surface pixel for given week was made up of the following individual fluxes:

$$s_{sf;i} = s_{ff\ week\ day;i} + s_{ff\ week\ night;i} + s_{ff\ weekend\ day;i} + s_{ff\ weekend\ night;i} + s_{NEE\ day;i} + s_{NEE\ night;i} \tag{6}$$

where $s_{sf;i}$ is the total weekly surface flux from the ith pixel, $s_{ff\ week\ day;i}$ is the fossil fuel flux during the day during the working week, $s_{ff\ week\ night;i}$ is the night-time fossil fuel flux during the working week, $s_{ff\ weekend\ day;i}$ is the weekend daytime fossil fuel flux, $s_{ff\ weekend\ night;i}$ is the weekend night-time fossil fuel flux, and $s_{NEE\ day;i}$ and $s_{NEE\ night;i}$ are the day and night-time NEE fluxes for the full week from the ith pixel. The inversion solved for each of these fluxes separately

10 and for each of the four weeks in the monthly inversion. Therefore a monthly inversion solved for $10,201 \times 6 \times 4 = 244,824$ surface fluxes. The mean day and night-time concentrations at each of the four domain boundaries for each week were the final components of the control vector. The inversion solved for $4 \times 2 \times 4 = 32$ boundary concentrations.

As a sensitivity analysis we examined two alternative approaches to the control vector. If we assumed that neither the NEE nor fossil fuel flux would change very much from week to week, an option would be to solve for the mean of the six

15 individual fluxes over the four weeks in a given month. We therefore considered a sensitivity test where the inversion solved for one average day and one average night NEE flux within each pixel, and four fossil fuel mean weekly fluxes (day and night working week, day and night weekend) (inversion **Mean Month**). We also considered performing a separate inversion for each week; i.e. four separate weekly inversions in place of each of the monthly inversions (inversion **Week**). In this case only the concentration measurements for one week were used and the individual weekly fluxes (two NEE and four fossil fuel) were

20 solved for, and this was repeated for each of the four weeks in the month. The benefit of these two alternative control vectors is that for each individual inversion the resulting $\mathbf{C}_{s_0}$ matrix is much smaller compared with the reference case.

When solving for only one week, or a mean weekly flux for a particular month, the number of surface sources reduced to $10,201 \times 6 = 61,206$. Solving for individual weeks required 4×2 additional boundary concentrations to be added to the control vector, and when solving for the mean weekly flux for the month, we allowed the boundary concentrations to differ for each

25 week, and therefore we still solved for the 32 boundary concentrations as in the reference case. Therefore the $\mathbf{C}_{s_0}$ for these two alternative control vectors is 16 times smaller than that of the reference inversion.

The benefit of these two alternative approaches is a substantial reduction (at least 75% reduction) in the time taken to perform the inversion. If the results are similar to that of the reference inversion, this type of saving in the computational time and resources would allow more components of the inversion to be tested in a shorter period of time.

30 ## 2.6 Sensitivity analysis approach

The sensitivity tests were divided into those which assessed alternative products for the prior information; those which assessed an alteration to the structure of the uncertainty covariance matrices; those which assess an alteration to the relative uncertainty specified in $\mathbf{C}_{s_0}$; those which assessed a homogenisation of a component of the prior information; those which considered

a simplified version of $\mathbf{C}_c$; and those which solved for an alternative control vector. A summary of the sensitivity tests are presented in Table 1.

The modelled concentrations from each inversion were compared with the observations by assessing the bias and standard deviation of the prior and posterior modelled concentration residuals. Residuals in the prior modelled concentrations were

5   calculated as:

$$\boldsymbol{c}_{res\,prior} = \boldsymbol{c} - \boldsymbol{c}_{mod\,prior}. \tag{7}$$

Residuals in the posterior modelled concentrations were calculated as:

$$\boldsymbol{c}_{res\,post} = \boldsymbol{c} - \boldsymbol{c}_{mod\,post}. \tag{8}$$

where $\boldsymbol{c}_{mod\,prior}$ are the CO_2 concentrations modelled from $\boldsymbol{s}_0$ and $\boldsymbol{c}_{mod\,post}$ are the CO_2 concentrations modelled from

10   the posterior estimate of $\boldsymbol{s}$, and $\boldsymbol{c}_{res\,prior}$ and $\boldsymbol{c}_{res\,post}$ are the respective residuals in the modelled concentrations. The bias, calculated as the mean of these residuals, and standard deviation of these residuals were provided for each inversion. We plotted the time series of the observed and modelled concentrations to assess the skill of the inversion to reproduce the observed concentrations, particularly "local events", which were periods of larger than normal spikes in the observed concentration signal.

15   The posterior fluxes from each inversion were compared with those of the reference inversion in a number of ways. The posterior flux estimates and their spatial distribution were assessed for each inversion by mapping the mean total weekly flux within each pixel for two months (May and September 2012). We calculated the total flux over the domain, and plotted these weekly total fluxes over time together with the uncertainty bounds. We also considered the total flux over the domain for each month. These total flux estimates are the nett flux resulting from the fossil fuel and NEE flux estimates solved for by the

20   inversion. The inversion induces negative correlations between the fossil fuel and NEE flux components from the same week and pixel. When the total flux is considered in a particular pixel, the uncertainty for the total flux will be lower than the sum of the uncertainties for the individual components due to the negative covariance terms. The size of these negative covariances will depend on the prior information specified in the inversion framework. The total estimate gives an indication of the central tendency which we can compare between inversions, and allows us to assess, for example, if the inversion is predicting the

25   region to be a nett source or a nett sink. The uncertainties of these posterior total estimates allow us to assess the confidence we can place around these totals, and how this compares to the estimate itself.

In order to assess the goodness-of-fit of the prior uncertainty covariance matrices $\mathbf{C}_c$ and $\mathbf{C}_{\boldsymbol{s}_0}$, the χ^2 statistic, as described in Tarantola (2005), was calculated:

$$\chi_1^2 = \frac{1}{\nu}(\mathbf{H}\boldsymbol{s}_0 - \boldsymbol{c})^T(\mathbf{H}\mathbf{C}_{\boldsymbol{s}_0}\mathbf{H}^T + \mathbf{C}_c)^{-1}(\mathbf{H}\boldsymbol{s}_0 - \boldsymbol{c}) \tag{9}$$

30   where ν is the dimension of the data space, which is the number of observations used in the inversion.

The squared concentration residuals from the inversion should follow the χ^2 distribution with degrees of freedom equal to the number of observations (Michalak et al., 2005; Tarantola, 2005). Dividing this statistic by the degrees of freedom should

yield a χ_1^2 distribution. We compared these statistics between the different inversions to assess the suitability of the uncertainties prescribed to the prior fluxes.

Table 1. Description of sensitivity tests performed on the Cape Town inversion. Only those aspects which are changed for the sensitivity test are indicated. Other fields are the same as those for the reference inversion.

Sensitivity test abbreviation	Prior NEE product	Prior Fossil fuel product	NEE error correlations	Observation error correlations	Fossil fuel uncertainties	NEE uncertainties	Observation errors	Control vectors
Ref	CABLE	Cape Town Inventory	Balgovind 1 km	Balgovind 1 hr	Cape Town Inventory Errors	CABLE NPP	2 ppm (day); 4 ppm (night) with wind condition and measurement variance inflation	Six individual weekly fluxes
Carbon Assess	Carbon Assessment Product					Carbon Assessment NPP		
ODIAC		ODIAC			ODIAC Estimates ×100 %			
NEE Corr				No observation error correlation				
Obs Corr			No NEE error correlation					
No Corr			No NEE error correlation	No observation error correlation				
Double FF					Cape Town Inventory Errors ×2			
Half FF					Cape Town Inventory Errors ×$\frac{1}{2}$			
Double NEE						CABLE NPP ×2		
Half NEE						CABLE NPP ×$\frac{1}{2}$		
Domestic Homogenised		Cape Town Inventory with domestic emissions homogenised over the year			Cape Town Inventory Errors domestic emissions homogenised			
NEE Homogenised	Averaged CABLE weekly estimates over all pixels					Averages CABLE NPP weekly estimates over all pixels		
Simp Obs Error							2 ppm (day); 4 ppm (night)	
Simp Obs with Large Night							2 ppm (day); 10 ppm (night)	
Simp Obs No Corr				No observation error correlation			2 ppm (day); 4 ppm (night)	
Mean Month								Six average weekly fluxes for each month
Week								Separate weekly inversions

3 Results

The results of the reference inversion (**Ref**) are explained in detail in Nickless et al. (2018). The following sections compare the sensitivity tests to **Ref** with respect to the modelled concentrations, pixel-level weekly flux estimates, and aggregated fluxes over each week, month and over the full measurement period. When we refer to the total pixel-level weekly flux, this is the sum

5 of the four weekly fossil fuel fluxes (week / weekend; day / night) and the two NEE fluxes (day and night) within that pixel. The uncertainty of this total flux is obtained by first obtaining the sum of all the error variance and covariance terms of these six fluxes, and then taking the square root of this total variance term. The aggregated total weekly flux is the sum of all these total fluxes over the full inversion domain for the week in question. The total uncertainty of this aggregated total flux is derived in the same way as for the pixel-level total weekly flux, but now summing over all variance and covariance terms applicable to

10 that week for all pixels in the domain.

Aggregated fluxes are often of interest. For example, we may wish to report the total flux for a region from year to year. As we did not have a contiguous measurement period covering all seasons or over a full year period, which is often reported in these city-scale inversions, we instead aggregated over weekly and monthly periods. The purposes of this is to illustrate how weekly fluxes estimated within the same monthly inversion may differ, and the differences in aggregated fluxes between

15 different inversions at different times of the year. These aggregated monthly fluxes are calculated in the same way as the aggregated weekly flux.

The biases in the prior and posterior modelled concentrations, together with the standard deviation of the residuals, are provided in Table 2. We supply the time series of the modelled concentrations for each inversion and at both sites in the Supplement (Sect. 1.1). We provide time series plots of the aggregated weekly fluxes and their uncertainty bounds (Supplement

20 Sect. 1.2) and a table of the aggregated monthly fluxes over the full domain for each month (Supplement Sect. 1.3). We also supply maps of the prior and posterior modelled fluxes, together with the uncertainty reduction in each pixel, in the supplementary material for the months of May (early winter) and September (spring / early summer) 2012 (Supplement Sect. 1.4). For the main paper we provide a table of the aggregated fluxes over the full inversion period, together with the uncertainty reduction in the aggregated flux estimate and the mean χ^2 statistic which provides an assessment of the appropriateness of the

25 prior covariance matrices (Table 3).

Table 2. Bias (ppm) in the prior and posterior modelled concentrations together with the standard deviation of the modelled concentration residuals at the Hangklip and Robben Island measurement sites for the period March 2012 to June 2013. NEE = Net Ecosystem Exchange, FF = Fossil Fuel

Hangklip						
	Ref	**Carbon Assess**	**ODIAC**	**NEE Corr**	**Obs Corr**	**No Corr**
Prior Bias (sd)	2.4 (17.6)	-4.8 (12.4)	-6.1 (27.8)	2.4 (17.6)	2.4 (17.6)	2.4 (17.6)
Posterior Bias (sd)	0.0 (2.5)	-0.4 (4.2)	-0.1 (2.1)	0.0 (2.5)	0.0 (2.9)	0.0 (2.9)
	Double FF	**Half FF**	**Double NEE**	**Half NEE**	**Domestic Homogenised**	**NEE Homogenised**
Prior Bias (sd)	2.4 (17.6)	2.4 (17.6)	2.4 (17.6)	2.4 (17.6)	3.2 (16.3)	2.1 (13.2)
Posterior Bias (sd)	0.0 (2.3)	0.1 (2.6)	0.0 (2.0)	0.1 (3.0)	0.1 (2.4)	0.0 (2.1)
	Simp Obs Error	**Simp Obs with Large Night**	**Simp Obs No Corr**	**Mean Month**	**Week**	
Prior Bias (sd)	2.4 (17.6)	2.4 (17.6)	2.4 (17.6)	2.5 (17.7)	1.2 (15.6)	
Posterior Bias (sd)	-0.1 (2.3)	-0.1 (2.3)	0.0 (2.9)	0.0 (2.5)	-0.1 (2.9)	
Robben Island						
	Ref	**Carbon Assess**	**ODIAC**	**NEE Corr**	**Obs Corr**	**No Corr**
Prior Bias (sd)	-2.9 (21.4)	-12.6 (20.1)	-17.1 (43.7)	-2.9 (21.4)	-2.9 (21.4)	-2.9 (21.4)
Posterior Bias (sd)	0.5 (3.9)	0.3 (5.2)	0.6 (3.6)	0.5 (3.7)	0.5 (4.2)	0.5 (3.9)
	Double FF	**Half FF**	**Double NEE**	**Half NEE**	**Domestic Homogenised**	**NEE Homogenised**
Prior Bias (sd)	-2.9 (21.4)	-2.9 (21.4)	-2.9 (21.4)	-2.9 (21.4)	-1.0 (20.2)	-6.4 (19.8)
Posterior Bias (sd)	0.5 (3.6)	0.3 (4.2)	0.4 (3.5)	0.6 (4.3)	0.5 (3.9)	0.4 (3.1)
	Simp Obs Error	**Simp Obs with Large Night**	**Simp Obs No Corr**	**Mean Month**	**Week**	
Prior Bias (sd)	-2.9 (21.4)	-2.9 (21.4)	-2.9 (21.4)	-3.5 (20.6)	-4.2 (18.5)	
Posterior Bias (sd)	0.1 (3.6)	0.1 (3.4)	0.0 (4.5)	0.6 (4.0)	0.5 (4.3)	

The sd alongside the bias refers to the standard deviation of the residuals of the modelled concentrations in units of ppm. Ref = Reference Inversion; Carbon Assess = Carbon Assessment Inversion; ODIAC = ODIAC fossil fuel inversion; NEE Corr = Correlation for NEE flux uncertainties only; Obs Corr = Correlation for observation errors only; No Corr = No correlation specified in prior covariance matrices; Double FF = Double fossil fuel uncertainties; Half FF = Half fossil fuel uncertainties; Double NEE = Double NEE uncertainties; Half NEE = Half NEE uncertainties; Domestic Homogenised = Domestic emission homogenised over the year; NEE Homogenised = NEE fluxes averaged over the domain; Simp Obs Error = Simple specification of observation error covariance matrix; Simp Obs with Large Night = Simple observation error covariance matrix with larger night-time error; Simp Obs No Corr = Simple observation error covariance matrix with no correlation; Mean Month = Inversion solving for mean weekly fluxes over the month; Week = Separate inversions for each week.

Table 3. Prior and posterior total flux estimates of each inversion over the thirteen four-week periods for which observation data were available from March 2012 to June 2013, with uncertainties and the reduction in uncertainty with respect to the prior uncertainty. Total fluxes are expressed as $\mathrm{kt}\ CO_2$. The mean χ^2 statistic is provided over the thirteen inversion periods. NEE = Net Ecosystem Exchange, FF = Fossil Fuel

	Ref	**Carbon Assess**	**ODIAC**	**NEE Corr**	**Obs Corr**	**No Corr**
Prior Flux (sd)	-1336 (254)	5181 (32)	7635 (256)	-1336 (254)	-1336 (63)	-1336 (63)
Posterior Flux (sd)	-317 (189)	4045 (28)	5787 (195)	-310 (189)	-1281 (59)	-1287 (59)
Uncertainty Reduction	25.6%	11.9%	23.6%	25.6%	7.5%	7.5%
Mean χ^2 Statistic	1.48 (0.55)	4.13 (1.24)	1.25 (0.49)	1.49 (0.54)	2.10 (0.78)	2.12 (0.79)
	Double FF	**Half FF**	**Double NEE**	**Half NEE**	**Domestic Homogenised**	**NEE Homogenised**
Prior Flux (sd)	-1336 (255)	-1336 (254)	-1336 (508)	-1336 (128)	-1916 (254)	-1328 (126)
Posterior Flux (sd)	-151 (190)	-423 (189)	-316 (365)	-337 (100)	-624 (189)	-1707 (106)
Uncertainty Reduction	25.4%	25.7%	28.2%	21.9%	25.6%	15.8%
Mean χ^2 Statistic	1.21 (0.50)	1.86 (0.63)	1.03 (0.47)	2.22 (0.69)	1.41 (0.49)	1.17 (0.47)
	Simp Obs Error	**Simp Obs with Large Night**	**Simp Obs No Corr**	**Mean Month**	**Week**	
Prior Flux (sd)	-1336 (254)	-1336 (254)	-1336 (254)	-1336 (126)	-1220 (251)	
Posterior Flux (sd)	-325 (188)	-579 (192)	-338 (188)	662 (66)	-687 (186)	
Uncertainty Reduction	26.1%	24.4%	26.1%	47.2%	25.8%	
Mean χ^2 Statistic	2.17 (1.04)	1.88 (0.92)	2.25 (1.13)	1.43 (0.55)	1.54 (0.56)	

Prior and Posterior Flux refer to the total flux from the domain over the thirteen four-week periods. The sd of the fluxes refers to the uncertainty in the total flux estimate. The sd of the χ^2 statistic refers to the standard deviation between the χ^2 statistics of the thirteen four-week period χ^2 Statistics. Ref = Reference Inversion; Carbon Assess = Carbon Assessment Inversion; ODIAC = ODIAC fossil fuel inversion; NEE Corr = Correlation for NEE fluxes only; Obs Corr = Correlation for observation errors only; No Corr = No correlation specified in prior covariance matrices; Double FF = Double fossil fuel uncertainties; Half FF = Half fossil fuel uncertainties; Double NEE = Double NEE uncertainties; Half NEE = Half NEE uncertainties; Domestic Homogenised = Domestic emission homogenised over the year; NEE Homogenised = NEE fluxes averaged over the domain; Simp Obs Error = Simple specification of observation error covariance matrix; Simp Obs with Large Night = Simple observation error covariance matrix with larger night-time error; Simp Obs No Corr = Simple observation error covariance matrix with no correlation; Mean Month = Inversion solving for mean weekly fluxes over the month; Week = Separate inversions for each week.

3.1 Alternative prior information products

The prior biases for both the inversion making use of the carbon assessment for prior NEE flux estimates and uncertainties (which we denote with the emboldened shorthand **Carbon Assess**), and the ODIAC fossil fuel inversion (**ODIAC**) were larger in magnitude and more negative than those of the reference inversion (**Ref**). This indicates that the prior modelled concentra-

5   tions of CO_2 from these two inversions were larger on average compared with the observations. The standard deviation in these residuals was larger compared with **Ref** (Table 2). A plot of the modelled concentrations shows that for all three inversions, the prior modelled concentrations only weakly followed the observed concentrations, with modelled concentrations at the Robben Island site too large, and too small at the Hangklip site (Figures 3 and 4). In the case of the **Carbon Assess** inversion the prior modelled concentrations were not underestimated as much as those from **Ref** at the Hangklip site. The χ^2 statistics indicated

10   that the inversion framework specified for the **Carbon Assess** inversion had uncertainties that were too small (Table 3). For **ODIAC**, the χ^2 statistics were slightly closer to one than those for **Ref**.

The prior total weekly fluxes were notably different compared with **Ref** (Figure 5). The carbon assessment product for NEE fluxes resulted in prior total weekly flux estimates that were always positive and which showed little variation over the year compared with the reference prior. The uncertainty bands were much narrower for the carbon assessment total flux estimates.

15   The resulting posterior weekly fluxes were very similar to the priors.

The ODIAC product for fossil fuel fluxes resulted in prior total weekly fluxes that had a similar pattern of weekly fluxes over time as those obtained by **Ref** (Figure 5), with more positive fluxes between March and June 2012 and March and June 2013, and negative or near-zero total weekly fluxes between August 2012 and February 2013. These summer-time negative fluxes were not as negative as those obtained by **Ref**.

20   Considering the aggregated flux for each month over the inversion domain, the **Carbon Assess** inversion had larger prior fluxes for every month compared with **Ref**, particularly during the summer months. During these months the discrepancy between the reference and carbon assessment prior aggregated fluxes was between 699 and 1386 kt CO_2 for a four week period (Supplement Sect. 1.3). The inversion reduced these fluxes. The resulting posterior fluxes were still larger than the reference posterior fluxes by between 400 and 1000 kt CO_2 for this same period. The ODIAC prior fluxes were always larger

25   than the reference priors, but consistently for all months by an amount of approximately 690 kt CO_2. The posterior aggregated fluxes were still larger than those for **Ref**, but the difference was reduced to 469 kt CO_2 on average.

Whereas the aggregated total prior fluxes from **Ref** were generally made more positive by the inversion, there were some months when the total fluxes were made more negative, notably during the winter months. In the case of the **Carbon Assess** inversion, fluxes were made more negative by the inversion for all months. The resulting posterior total fluxes were positive for

30   all months. For **ODIAC**, the posterior fluxes were more negative than their priors, indicating that compared with the reference, the positive fluxes from the fossil fuel sources were specified too large. August and September 2012 were the only months when **ODIAC** made the total posterior fluxes larger than the priors, which agrees with the direction in which **Ref** adjusted the posterior total fluxes.

The aggregated total fluxes of these alternative prior product inversions over the thirteen inversion periods are larger than for **Ref** (Table 3). The uncertainty of the aggregated total flux for **Carbon Assess** was smaller relative to **Ref**, whereas **ODIAC** obtained similar uncertainties in the aggregated total flux. The corrections made by the inversion made the aggregated total flux of **Ref** less negative and closer to zero. When these two alternative prior products were used, the inversion corrected

5   the prior fluxes to be less positive, also attempting to make these fluxes closer to zero. The uncertainty reduction achieved over the full inversion period was 25.6% for **Ref** and 23.6% for **ODIAC**, but only 11.9% for **Carbon Assess**. This smaller uncertainty reduction is due to prior biospheric flux estimates from the carbon assessment product being close to zero, with corresponding small NPP fluxes, and therefore error correlations much smaller in comparison with **Ref**. The error correlations play an important role in determining the uncertainty reduction achievable by the inversion.

10   The spatial distribution of the prior and posterior fluxes for May 2012 are provided in Figure 6. **Carbon Assess** has prior total flux estimates that are notably closer to zero and less negative compared with **Ref** across both May and September 2012 (provided in the Supplement Sect. 1.4). **Ref** was able to change the spatial distribution of these negative fluxes somewhat, but still maintained these negative fluxes in the posterior estimates. The posterior fluxes of **Carbon Assess** were largely left unchanged, with September 2012 having the most notable adjustments with a small area of negative fluxes created to the east

15   of the oil refinery pixel, to the north of the Cape Town metropolitan area.

The map of the ODIAC prior fluxes is distinctly different to those of **Ref** (Figure 6). The reference inventory limited the fossil fuel fluxes to a few specific pixels, with a small number of pixels over point sources with large positive fluxes. The ODIAC product smoothed the fluxes over the Cape Town metropolitan area, covering a larger area with positive fluxes compared with the reference case, and having only three pixels with distinctly larger fluxes than the rest of the region. Although the ODIAC

20   priors do not show any of the very large positive fluxes of the reference, the area of positive flux resulting from the fossil fuel fluxes is focused on the same general area as **Ref**.

With regards to the uncertainty reduction (Figure 6), **Ref** was able to obtain higher reductions than either of these test cases. The spatial pattern of uncertainty reduction was similar between **ODIAC** and **Ref**, whereas for **Carbon Assess** many of the pixels in the domain showed no uncertainty reduction.
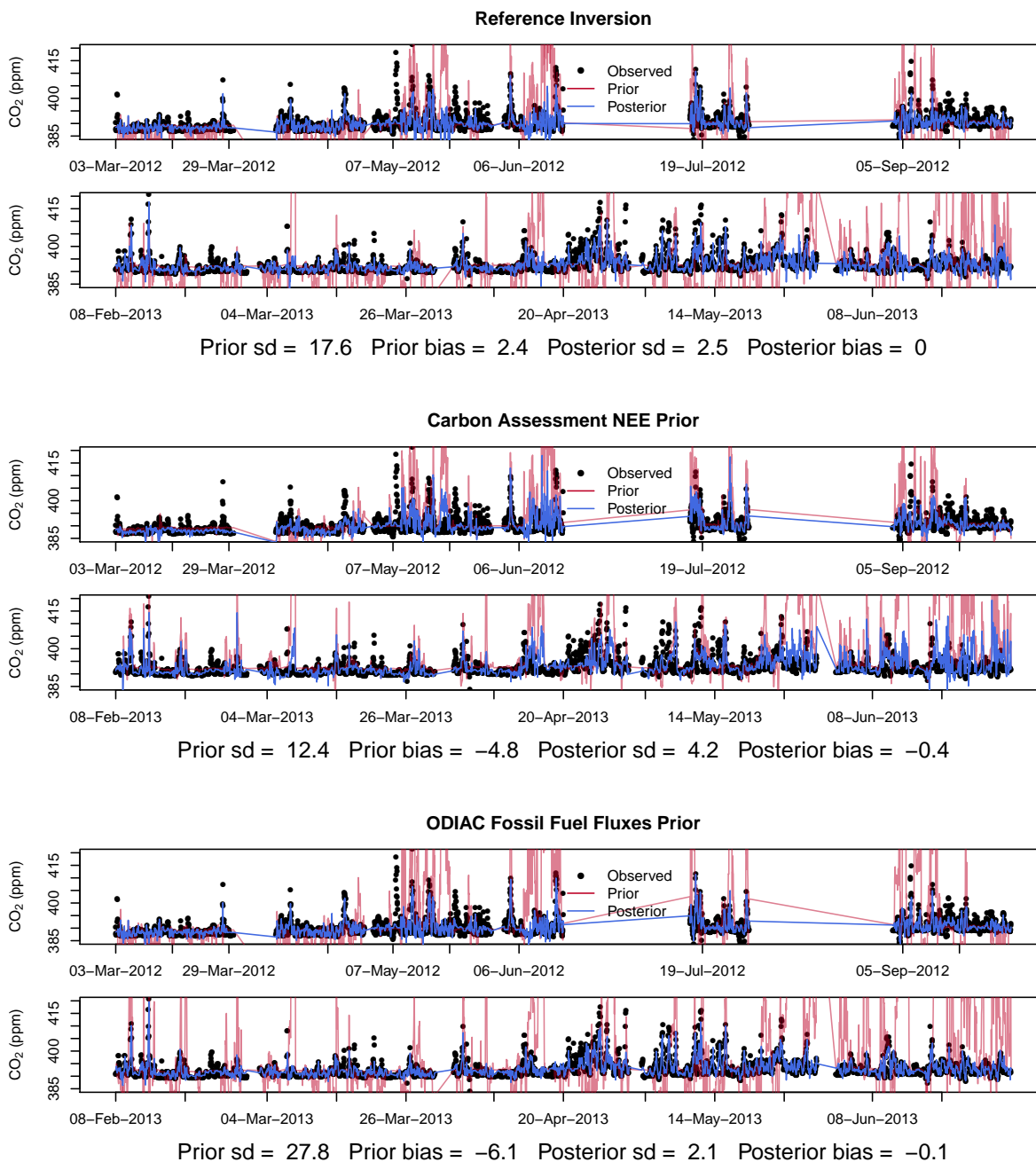
Figure 3. Prior and posterior modelled concentrations for the Hangklip site over the full inversion period from March 2012 until June 2013 for the reference inversion (top), carbon assessment inversion (middle), and ODIAC fossil fuel flux product inversion (bottom).
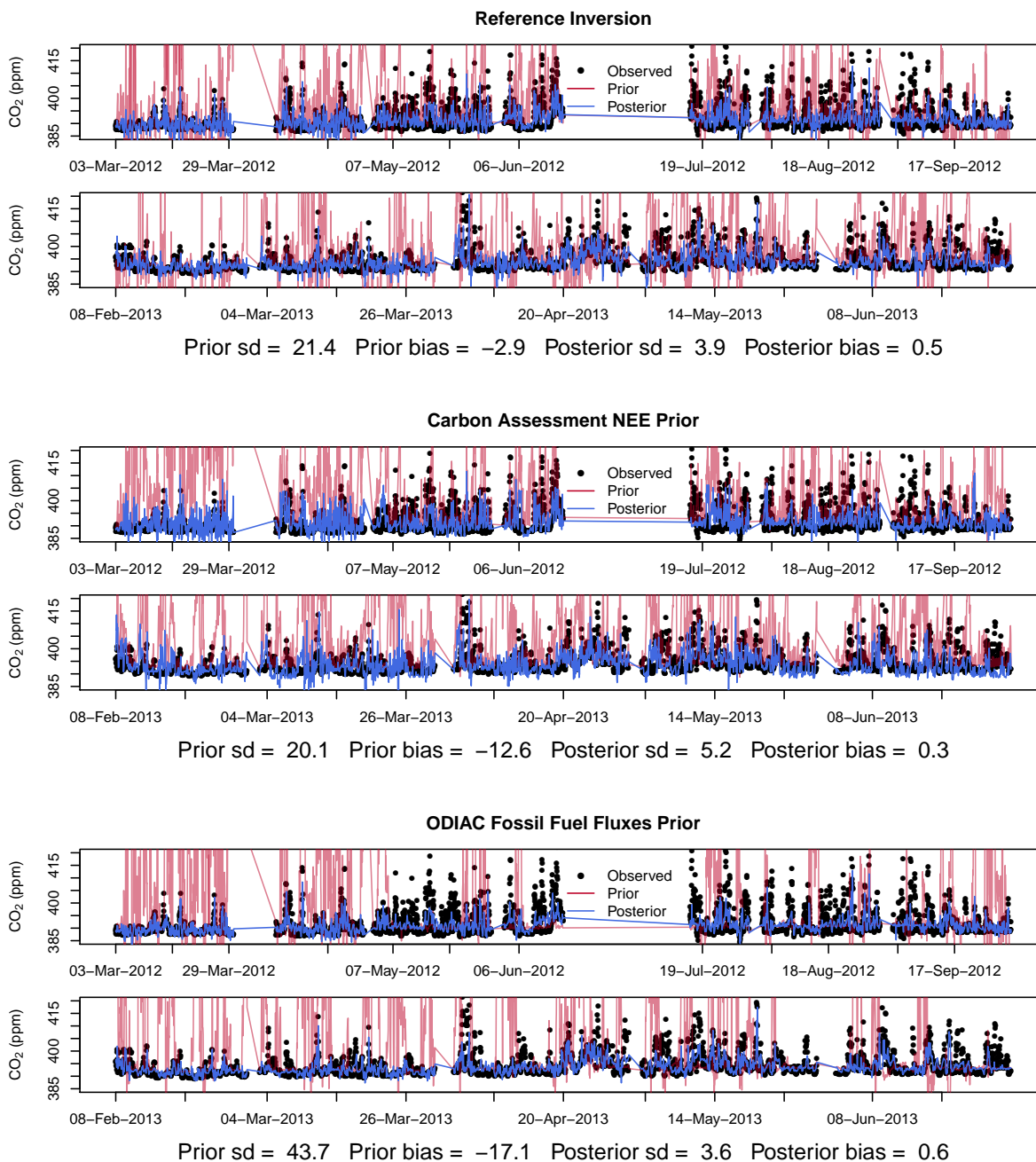
Figure 4. Prior and posterior modelled concentrations for the Robben Island site over the full inversion period from March 2012 until June 2013 for the reference inversion (top), carbon assessment inversion (middle), and ODIAC fossil fuel flux product inversion (bottom).
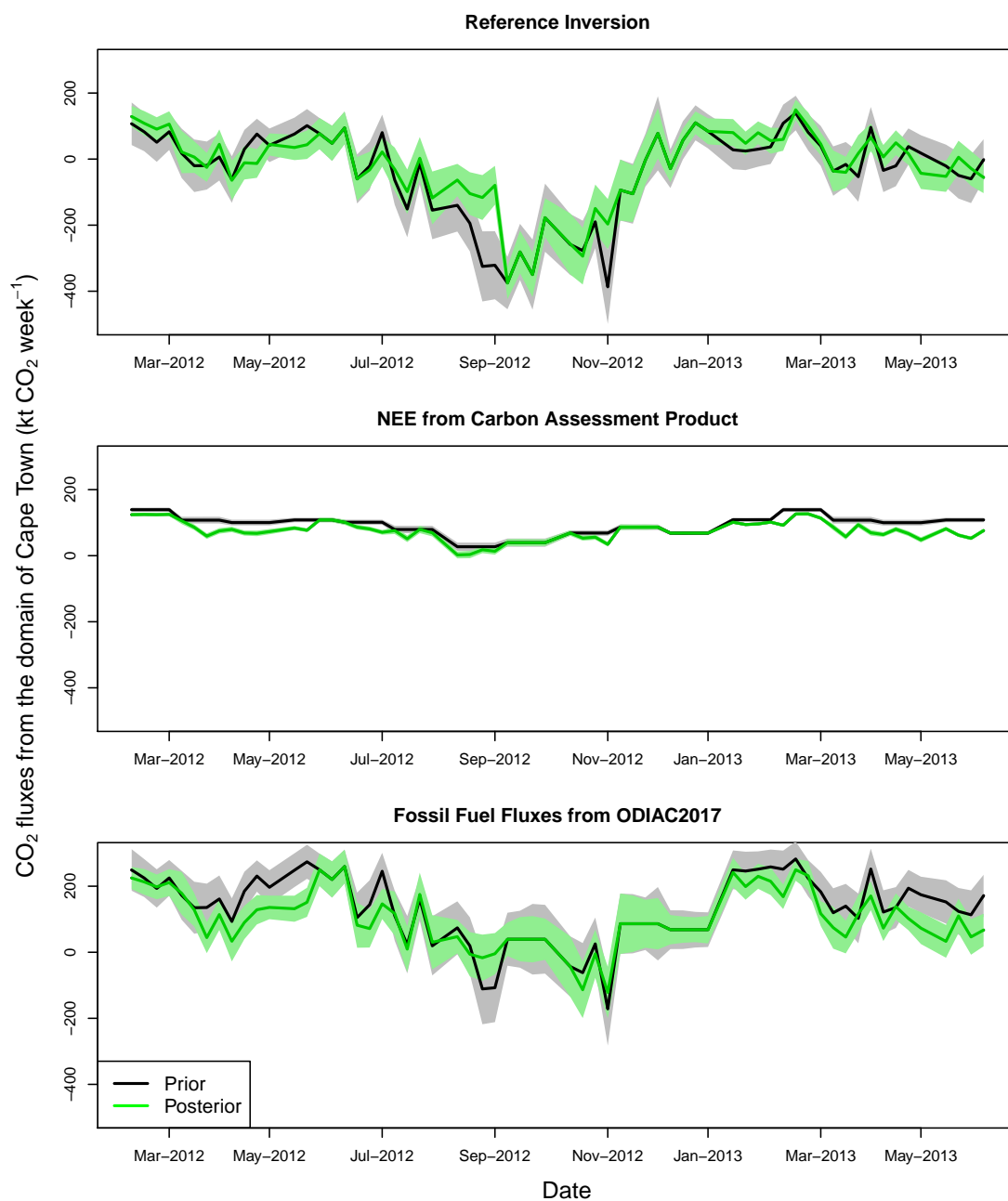
Figure 5. Prior and posterior aggregated weekly fluxes over the inversion domain from March 2012 to June 2013 for the reference, carbon assessment and ODIAC inversions.
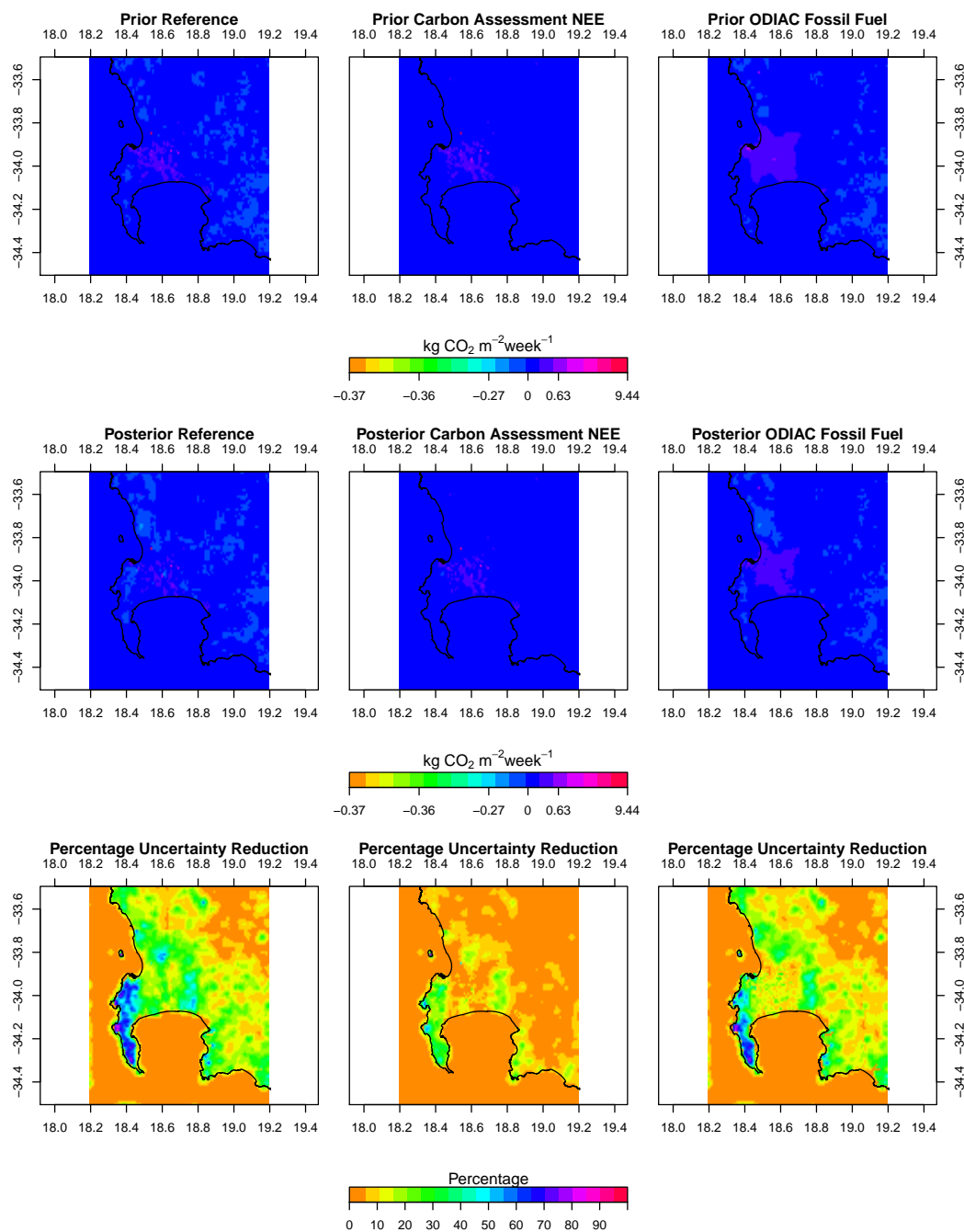
Figure 6. Spatial distribution of the prior (top row) and posterior (middle row) total weekly fluxes in May 2012 for the reference (left column), carbon assessment (middle column) and ODIAC (right column) inversions, as well as the uncertainty reduction achieved at the pixel-level relative to the prior uncertainty (bottom row).

3.2 Uncertainty covariance matrix structure: $\mathbf{C}_{s_0}$ and $\mathbf{C}_c$

Ref accounted for correlation between the uncertainties in pixel-level NEE fluxes in space, as well as for temporal correlation in observation errors. The correlation lengths were made small in **Ref**. In this group of sensitivity tests, we assessed how the inversion results would be affected if we systematically ignored these sources of correlation.

In terms of the prior and posterior modelled concentrations achieved by these inversions, the bias and standard deviation in the model concentration residuals were similar (Table 2). The posterior modelled concentrations from those inversions which ignored NEE flux uncertainty (inversions **Obs Corr** and **No Corr**) had higher standard deviations in their residuals. The χ^2 statistics indicated that the inversion ignoring the observation error correlations (**NEE Corr**) had similar goodness-of-fit for the prior uncertainty covariance matrices as **Ref**, but that the two inversions that ignored the spatial correlation between NEE flux uncertainties had poorer goodness-of-fit (Table 3). The χ^2 statistics for these latter two inversions were as high as 3.3, as for the inversion in July. In comparison, the removal of the temporal correlation in the observation errors had only a small penalty in the χ^2 statistic.

In **Ref**, the positive covariances specified between neighbouring NEE flux uncertainties led to large prior and posterior uncertainty around the aggregated weekly fluxes. For the test cases with observation error correlation only or no correlation at all, the uncertainty bounds around the prior and posterior aggregated fluxes are indistinguishable from **Ref**. If these positive covariances are removed from $\mathbf{C}_{s_0}$ then the uncertainty around the aggregated total flux was much smaller.

When aggregating over a month, ignoring NEE flux uncertainty correlations made a large difference to the aggregated monthly flux as well as to its uncertainty. The posterior aggregated fluxes for each month were similar to the priors in these two test cases, and the uncertainty reduction was very small. For **Ref** and **NEE Corr**, the uncertainty reduction in the monthly aggregated flux was on average 26.6% whereas for the **Obs Corr** and **No Corr** the uncertainty reduction was on average only 7.6%. Aggregating over the full period leads to estimates of -317 and -310 kt CO_2 for **Ref** and **NEE Corr**, whereas **Obs Corr** and **No Corr** had posterior estimates of -1281 and -1287 kt CO_2, close to the prior aggregated fluxes (Table 3).

The spatial distribution of the posterior fluxes were similar for **Ref** and **NEE Corr**. The spatial distribution changed when these NEE covariances were removed. The adjustments made to the pixel-level fluxes in these inversions were small and limited to only a few pixels, whereas in **Ref** adjustments were made to larger areas of the domain. The uncertainty reductions achieved by **Obs Corr** and **No Corr** were small and confined to only a few pixels, with a much larger proportion of the domain showing no uncertainty reduction in comparison with **Ref** (Figure 7).
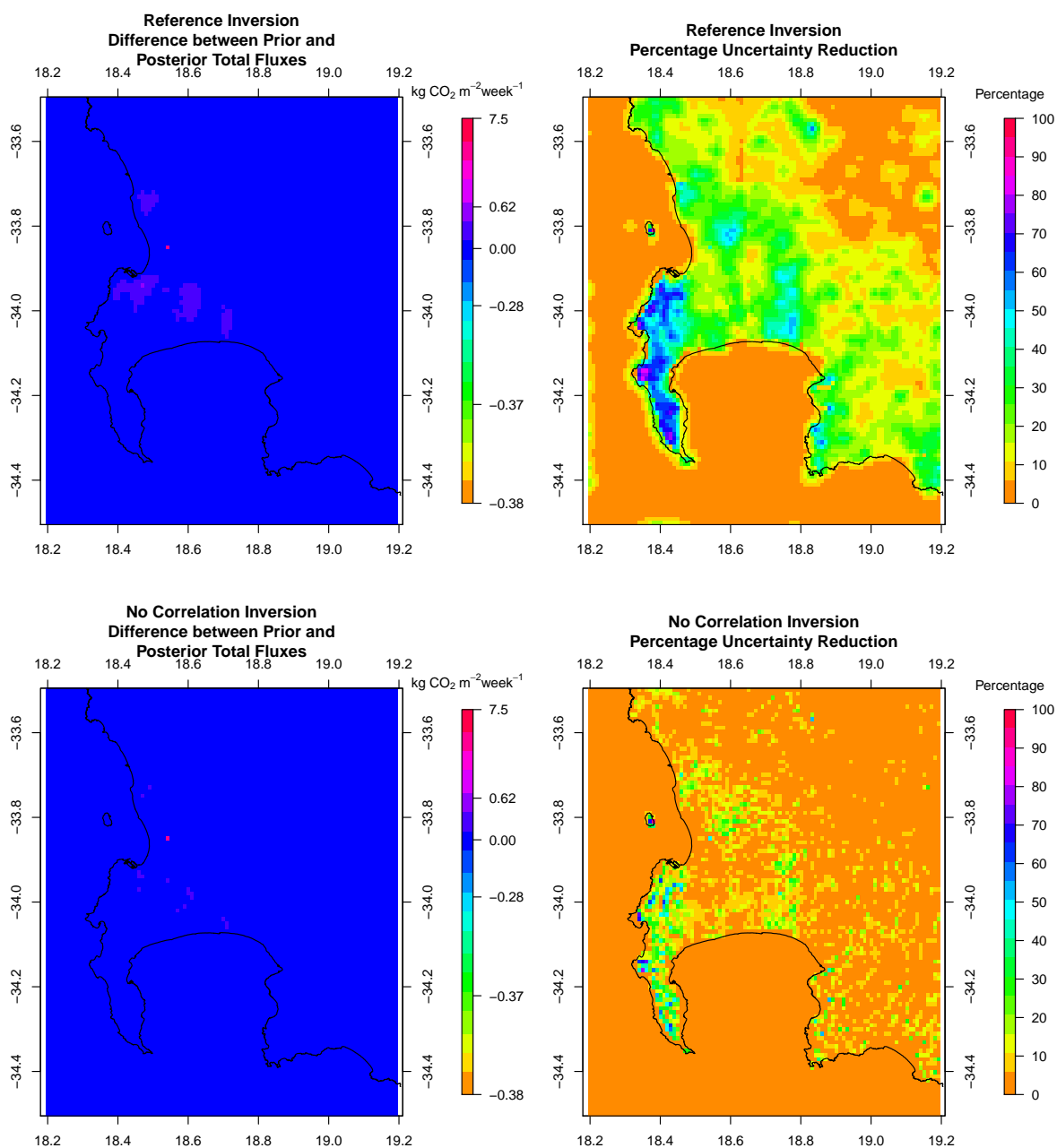
Figure 7. Spatial distribution in the adjustments made by the inversion to the prior fluxes in May 2012 for the reference inversion (top left), and no correlation inversion (bottom left), as well as the uncertainty reduction achieved at the pixel-level relative to the prior uncertainty (right).

3.3 Relative uncertainty in C_{s_0}

In this group of sensitivity tests we assessed how the relative contribution of the uncertainty in the fossil fuel and NEE fluxes affected the inversion results. We considered doubling and halving these uncertainties with respect to **Ref** uncertainties. The impact on the modelled concentrations was small. Biases were similar to **Ref** at both sites, and the standard deviation in the

5   residuals of the modelled concentrations were similar (Table 2). The χ^2 statistics were larger when the uncertainties were halved, particularly the uncertainties in the NEE fluxes (inversion **Half NEE**), indicating that insufficient uncertainty had been assigned to either the fluxes or observations, whereas doubling the uncertainties led to χ^2 statistics closer to one (Table 3).

The pattern in prior and posterior aggregated fluxes was similar between **Ref** and these test cases. The uncertainty around the weekly aggregated fluxes was strongly dependent on the NEE uncertainty (Table 8) (inversions **Double NEE** and **Half**

10   **NEE**), whereas it was not noticeably different if the uncertainty in the fossil fuel fluxes was either double or halved (inversions **Double FF** and **Half FF**).

In this group of sensitivity tests, the differences in the aggregated monthly fluxes was more pronounced between months within the same inversion than between inversions performed for the same month. All inversions corrected the prior aggregated fluxes to a similar degree and in the same direction. Doubling the uncertainty in the fossil fuel fluxes led to posterior aggregated

15   fluxes that were consistently larger for all months compared with **Ref**, whereas halving this uncertainty led to smaller posterior fluxes. Doubling and halving the uncertainty in the NEE fluxes led to posterior flux estimates that were similar on average to those of **Ref** but with greater variability in this difference between the reference and test inversion posterior estimates from month to month compared with the fossil fuel test inversions.

Double NEE obtained the largest uncertainty reduction, but the resulting posterior uncertainty was larger than for **Ref**.

20   Halving the NEE uncertainty led to smaller relative uncertainty reductions for the aggregated monthly fluxes, and therefore posterior uncertainties that were similar in magnitude to the prior uncertainties. The uncertainties in the posterior aggregated monthly fluxes were similar between **Ref**, **Double FF**, and **Half FF**. It was always higher for **Double NEE**, and lower for **Half NEE**. The resulting uncertainty in the posterior aggregated flux for **Half NEE** was more similar to **Ref** than **Double NEE**. The aggregated flux over the full inversion period shows that, whereas this estimate was close to the result for **Ref** in

25   the case of the two NEE uncertainty cases (316 and 337 kt CO_2), the aggregated flux was more positive when the fossil fuel uncertainty was doubled (-151 kt CO_2) and more negative when the fossil fuel flux was halved (-423 kt CO_2) (Table 3). On the other hand, changing the relative uncertainty of the fossil fuel fluxes had no impact on the uncertainty in the posterior flux estimate, whereas doubling or halving the uncertainty in the NEE fluxes led to roughly doubling or halving the uncertainty in the posterior aggregated flux.

30   The spatial distributions of the posterior fluxes were similar between the inversions in this group of sensitivity tests. A notable feature in the September 2012 posterior fluxes is, when NEE uncertainty was doubled, the inversion was able to reduce the aggregated flux with respect to the priors, by creating a region of negative flux in an area close to the oil refinery point source to the north of the CBD region (Supplement Figure S42).
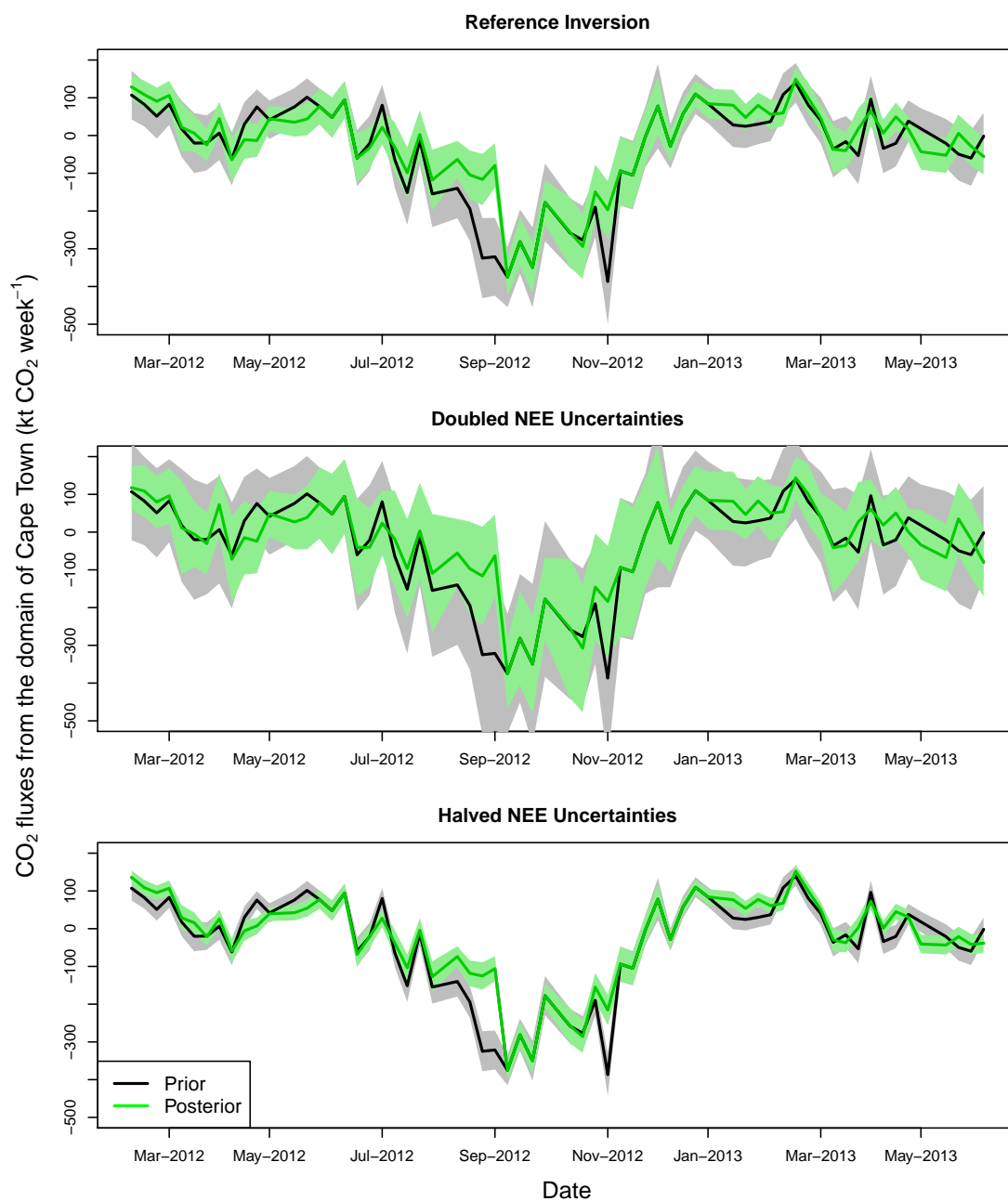
Figure 8. Prior and posterior aggregated weekly fluxes over the inversion domain from March 2012 to June 2013 for the reference inversion and the doubled and halved NEE uncertainty test cases.

3.4 Homogenised prior information

In this group of sensitivity tests we looked at the impact on the inversion results of assuming that the domestic emissions were constant through time (**Domestic Homogenised**), and of assuming a spatially homogeneous biogenic flux over the inversion domain within each month (**NEE Homogenised**). The prior modelled concentrations from these two test cases were biased to a

5   similar degree as **Ref**. Homogenising the NEE flux over space led to smaller standard deviations in the prior residuals. The most noticeable difference in the bias was for the Robben Island site, where the modelled concentrations under the homogenised NEE prior were biased by -6 ppm compared with the -3 ppm of **Ref**, indicating that prior fluxes around Robben Island (generally from the Cape Town central business district area and the Table Mountain National Park area adjacent to this region) were too positive (Table 2). The χ^2 statistics indicated that the inversion framework for these homogenised prior test cases

10   is more suitable than the reference case (Table 3). For the **NEE Homogenised** priors, the statistic was close to one for most months.

    The prior and posterior modelled concentrations for **Domestic Homogenised** are similar to those of **Ref**. In the case of **NEE Homogenised**, the time series shows better agreement between the prior modelled and observed concentrations at the Hangklip site, but worse agreement with respect to **Ref** at the Robben Island site (Figure 9).

15   There was no notable difference in the prior and posterior weekly aggregated flux between **Domestic Homogenised** and **Ref**. Smoothing NEE over space resulted in less extreme prior NEE and NPP estimates, and therefore the uncertainty around the NEE estimates was smaller than for **Ref**, leading to smaller uncertainties around the aggregated flux (Figure 10). The general pattern in the aggregated weekly fluxes over the course of the inversion period was similar to **Ref**.

    Compared to other groups of sensitivity tests performed here, the aggregated monthly fluxes were not very different between

20   the reference and test cases. For **Domestic Homogenised**, the adjustments made to the prior fluxes by the inversion were generally in the same direction and to the same degree as for **Ref**. The adjustments made by **NEE Homogenised** were not always in the same direction. The resulting posterior fluxes from **NEE Homogenised** were generally more negative than those of **Ref**. This is illustrated in the posterior aggregated fluxes for the inversion period (Table 3).

    Differences between the prior and posterior fluxes were small for **Ref** and these changes are consistent with those obtained

25   by **Domestic Homogenised**. In May 2012, which would have had a smaller domestic emissions specified than in **Ref**, the differences between the prior and posterior fluxes were limited to very few pixels, mainly near the Cape Town CBD area. In September 2012, when the domestic emissions would have been larger than those for **Ref**, the adjustments made by the inversion were more widespread.

    When NEE was smoothed over the domain with each month, the adjustments made to the prior fluxes were very small

30   in comparison to **Ref**. Changes were restricted to a few pixels in the CBD region and close to the measurement sites. The uncertainty reduction was concentrated in the regions around the measurement sites and reached over 90% in these areas. Over the Table Mountain National Park, which had some of the highest uncertainty reductions in **Ref**, uncertainty reduction was limited to between 20 to 30% and almost no adjustment to these prior fluxes were made by the inversion (Figure 11).
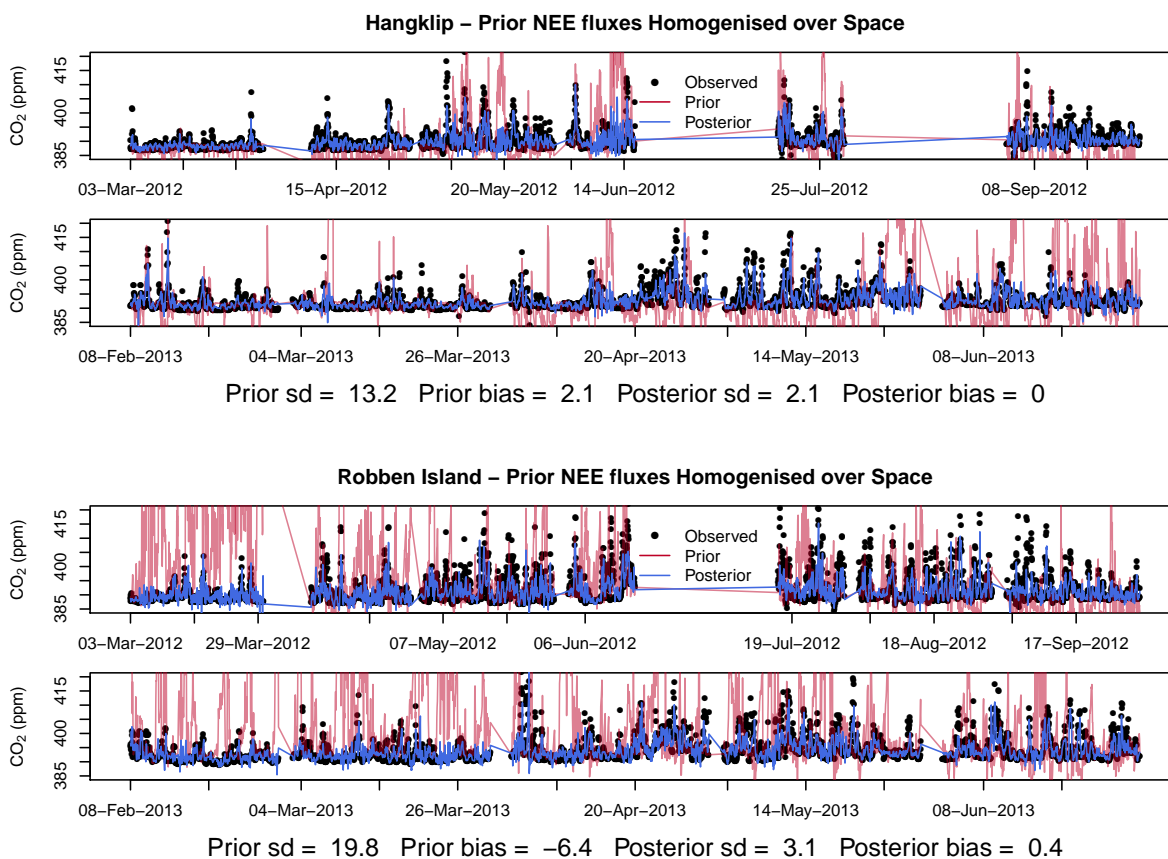
Figure 9. Prior and posterior modelled concentrations when the homogenised NEE prior was used for the Hangklip and Robben Island sites over the full inversion period from March 2012 until June 2013.
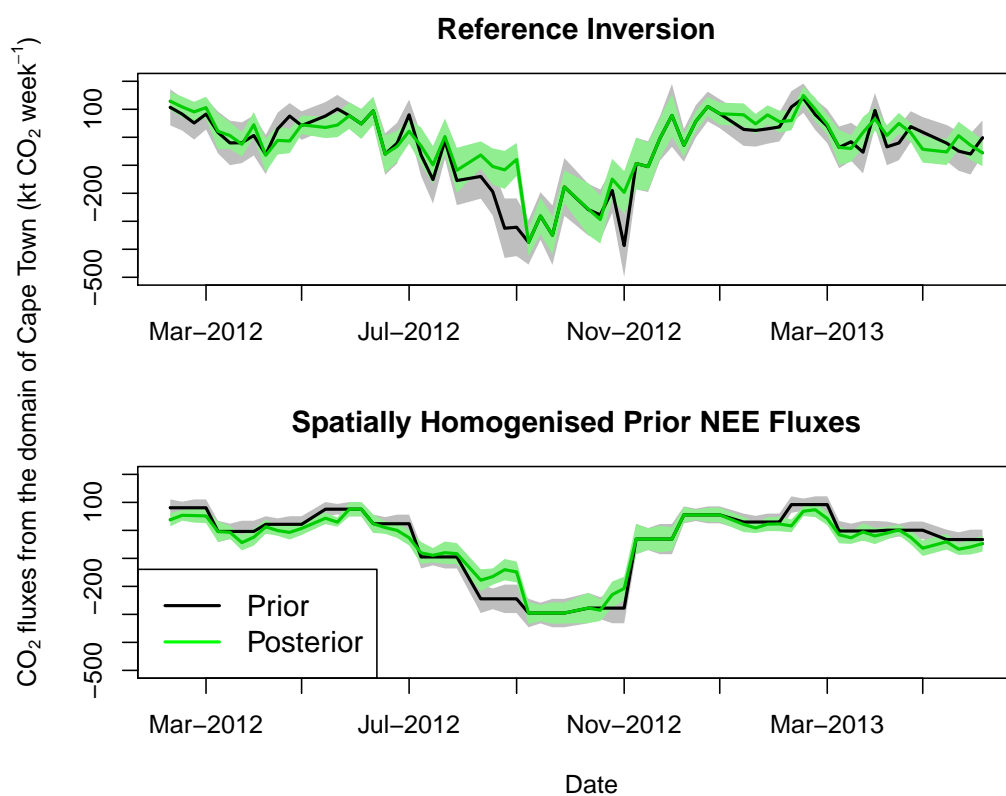
Figure 10. Prior and posterior aggregated weekly fluxes over the inversion domain from March 2012 to June 2013 for the reference inversion and homogenised NEE prior test case.
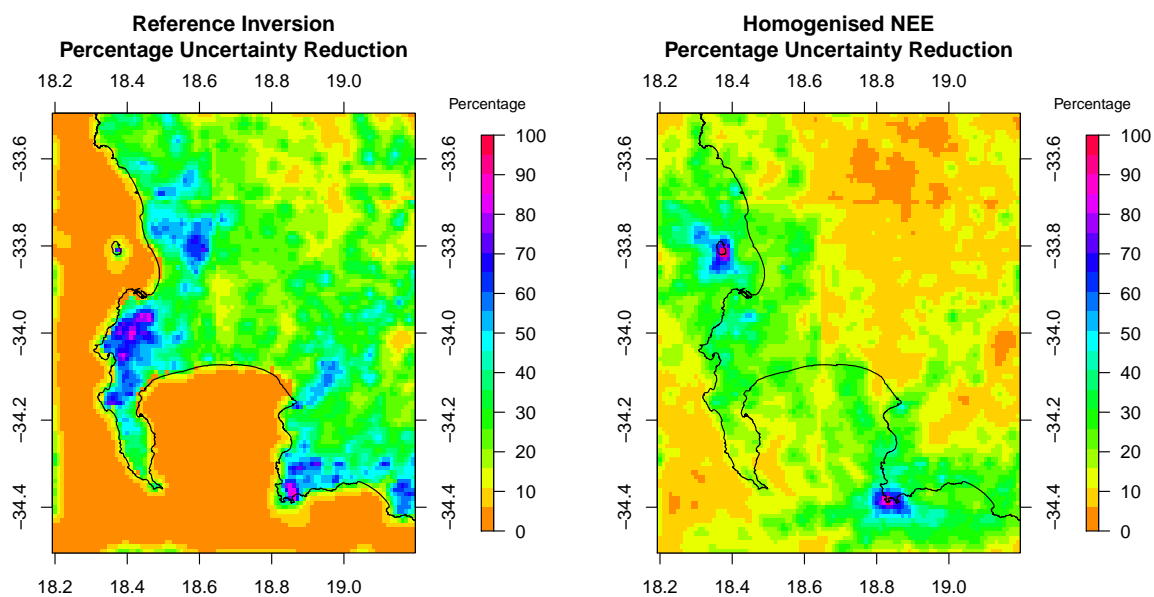
Figure 11. Spatial distribution of the pixel-level uncertainty reductions achieved by the reference inversion and homogenised NEE prior test case for September 2012.

3.5 Simplified C_c

In this group of sensitivity tests, the specification of C_c was simplified to a single uncertainty value of 2 ppm during the day or 4 ppm at night (**Simp Obs Error**), or up to 10 ppm for the night-time observations (**Simp Obs with Large Night**). These test cases had uncertainties in the observation errors that were lower than for **Ref**. Removing the correlation assumed in **Ref**

5 was also considered (**Simp Obs No Corr**). The χ^2 statistics indicated that simplifying the C_c with smaller errors reduced the goodness-of-fit of the prior uncertainty covariance matrices (Table 3).

The impact on the modelled concentrations was very small, with biases in the prior and posterior modelled concentrations closes to those obtained by **Ref** (Table 2). The bias for the Robben Island modelled concentrations was slightly reduced compared with **Ref** in all three of the simple observation error test cases.

10 The posterior aggregated weekly fluxes of the simple observation error cases and their uncertainties were indistinguishable from those of **Ref**. The posterior fluxes, both the spatial distribution in these fluxes and the aggregated fluxes, were similar between all three test cases and when compared with **Ref**. The uncertainty reduction was slightly larger under the simplified (i.e. smaller) observation error covariance matrix, but the spatial distribution in the uncertainty reduction was the same. Increasing the night-time observation errors to account for greater uncertainty in the atmospheric transport at night led to an aggregated

15 flux estimate over the full measurement period that was more negative than for **Ref**, but with a similar uncertainty in the posterior aggregated flux (Table 3). The aggregated fluxes for this test case were consistently more negative across all months compared with **Ref**. Removing the correlation between observation errors had little impact on the inversion results.

3.6 Alternative control vectors

Performing separate weekly inversions (**Week**) or solving for a mean weekly flux for the month (**Mean Month**) led to in-

20 versions that required less computational resources and time, which meant these inversions could be completed for the full inversion period faster than **Ref**.

The time series in the posterior modelled concentrations, and the bias and standard deviation in the posterior modelled concentrations were similar between **Ref** and the two alternative control vector inversions (Table 2). The χ^2 statistics were similar for these three inversions.

25 **Ref** and **Week** had similar aggregated weekly fluxes (Supplement Sect. 1.2). For **Mean Month**, the weekly aggregated fluxes were forced to be the same within each month, but the general pattern over time was similar to **Ref**. For most months the posterior weekly flux was above or below the prior weekly flux to the same degree as **Ref**, but the estimates, as expected, were smoother over time.

The monthly aggregated fluxes were generally very close to those from **Ref** except for August, September and November

30 2012 (Supplement Sect. 1.3). These are the summer months, and there was a great deal of variation in the aggregated fluxes from week to week from the results of **Ref** in these months. **Mean Month** generally had aggregated fluxes that were closer to zero than **Ref** or **Week**. This had a large impact on the aggregated flux over the full measurement period, due to these less negative posterior aggregated fluxes during the summer months. The aggregated flux for **Mean Month** was 662 kt CO_2 compared with

the -317 kt CO_2 of **Ref** (Table 3). **Week** had an aggregated flux of -687 kt CO_2. This discrepancy is partly due to some weeks with missing observations. In **Ref** these fluxes would have been adjusted by the available observations for neighbouring weeks, but were completely unconstrained by the observations in **Week**. For those months when all measurements were available, the aggregated totals were similar between **Ref** and **Week**. The uncertainty reduction in the aggregated estimates was almost

5   double for **Mean Month** compared with **Ref** and **Week**.

The spatial distribution of the posterior fluxes was very similar for **Ref** and **Week**, but was distinctly different for **Mean Month**. Notably, the area around the oil refinery pixel was adjusted to negative fluxes for the month of September (Figure 12). Other areas were made closer to zero compared with **Ref**. For the month of May the posterior fluxes in the CBD were distributed differently and a new area of relatively large negative fluxes was created north west of the oil refinery pixel (refer

10   to Supplement Figure S55). The uncertainty reductions at the pixel-level were large for the **Mean Month** compared with **Ref**, with areas of large uncertainty reduction much more widespread. In particular, the areas of uncertainty reduction above 90% that were restricted to the area over Table Mountain National Park in **Ref** were now extended over the CBD area.

Consequently the aggregated fluxes had uncertainty reduction that were twice as large as those for **Ref**, and uncertainties in the aggregated fluxes that were much smaller. For the aggregated flux over the full period, the posterior uncertainty was 66 kt

15   CO_2 for **Mean Month**, compared with the uncertainty of 189 and 186 kt CO_2 from **Ref** and **Week** respectively (Table 3).
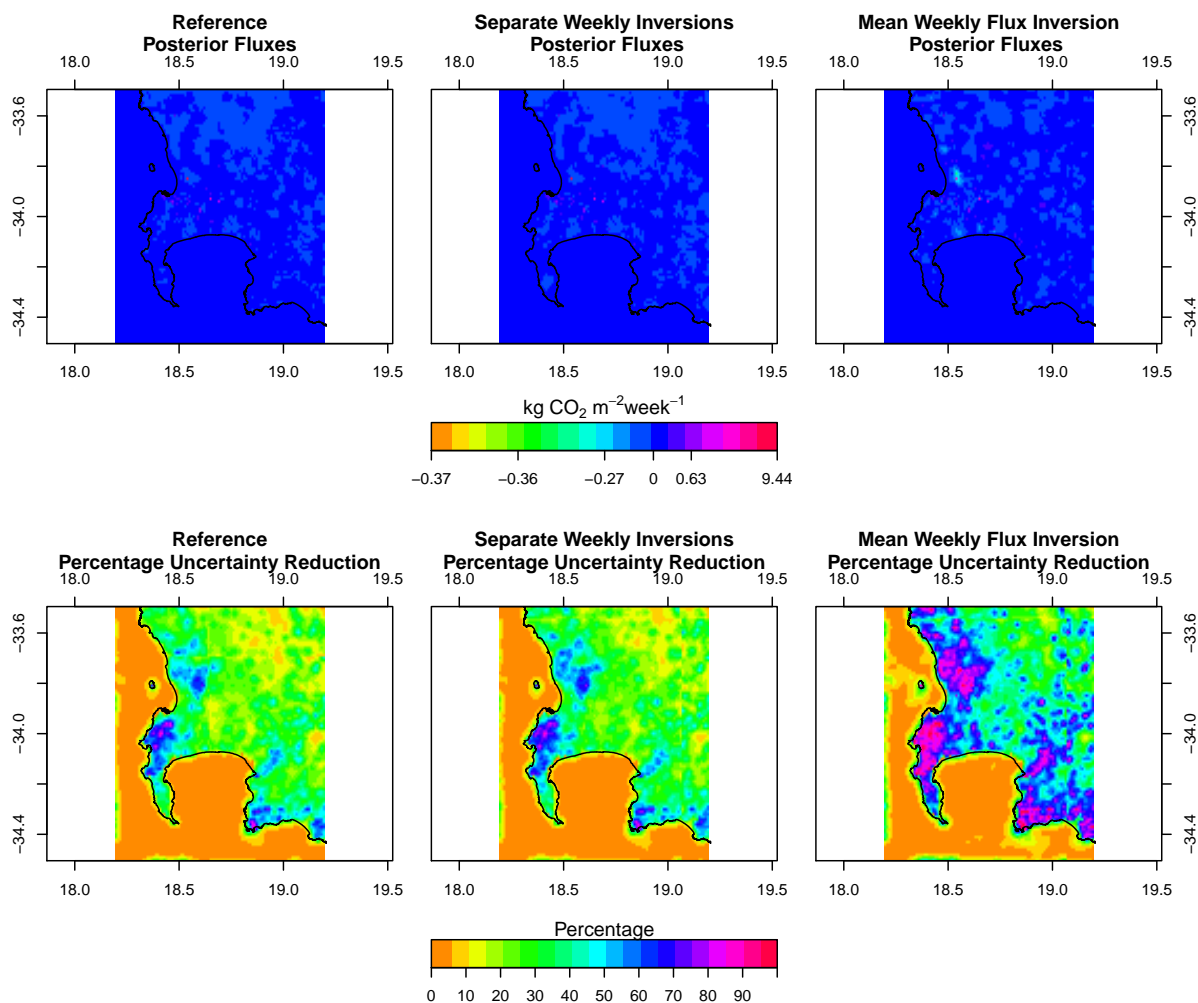
Figure 12. Spatial distribution of the pixel-level uncertainty reductions achieved by the reference inversion and homogenised NEE prior test case for September 2012.

4 Discussion

4.1 Alternative prior information products

As Robben Island is dominated by fossil fuel influence from the Cape Town metropolitan area, and Hangklip by biogenic sources from natural and agricultural areas in its vicinity, the discrepancy in the modelled concentrations relative to the observations suggests that the fossil fuel fluxes provided by the prior products are too large in magnitude, and the NEE estimates from CABLE estimate too much carbon uptake by the biota around the Hangklip site. In the case of the carbon assessment inversion, the bias in the prior modelled concentrations was positive compared with the negative bias of the reference inversion, indicating that the carbon assessment product was underestimating the uptake by the biota. As the carbon assessment product was much more homogeneous over space than CABLE, and could not react to local climate conditions, the uncertainty prescribed by using the NPP estimates is most likely too small.

The comparison of inversion results using different prior products provides useful information regarding which direction the true flux estimates are likely to be. A pixel within the CBD limits had similar fossil fuel flux estimates from the ODIAC product compared with the reference inventory product. The ODIAC product extended the fossil fuel fluxes much further a field from the CBD region than the reference inventory. This led to aggregated estimates that were much larger under the ODIAC inversion than the reference inversion. The inversion attempted to reduce the aggregated flux, indicating that compared with the reference inventory, the ODIAC prior was most likely overestimating the amount of fossil fuel emissions from Cape Town. Combining the information from these two inversions would imply that the true flux is sandwiched between the upper limit of the reference inversion and the lower limit of the ODIAC inversion; a much narrower uncertainty region than for either inversions. It can therefore be deduced that the true fossil fuel flux lies somewhere between the reference inventory and ODIAC fossil fuel flux estimates.

4.2 Uncertainty covariance matrix structure: $\mathbf{C}_{s_0}$ and $\mathbf{C}_c$

From the analysis of the reference inversion (Nickless et al., 2018), the χ^2 statistics indicated that the reference inversion could be improved by small increases to the uncertainty specified in $\mathbf{C}_{s_0}$, either through accounting for a larger correlation length or increasing the pixel-level uncertainties. Removal of the observation error correlations had a very small impact on the goodness-of-fit statistics, or on the posterior flux estimates and uncertainty reduction achieved by the inversion. To ensure that our reference inversion did not deviate too far from conventions for city-scale inversions where observation error correlations are ignored, we assigned a very short error correlation length to the observations of one hour. If we had assigned a longer length, such as 6 hours, this may have had more of an effect on the inversion. Lauvaux et al. (2009) have shown that observation errors up to 24 hours apart may be strongly correlated. The specification of the most suitable observation error length is still under investigation.

The impact of the inversion on the posterior fluxes and their uncertainties strongly depended on the specification of the correlation between the uncertainties in the NEE fluxes. In particular, the aggregated fluxes were distinctly different between the reference and test cases ignoring covariances between NEE flux uncertainties, which tended to have aggregated fluxes

closer to the priors and uncertainty reductions achieved by the inversion that were much lower (7.6% compared with 26.6% on average by the reference inversion). This indicates that advantage should be taken of knowledge related to the correlation induced by homogeneity of biogenic productivity in subregions of the domain. If this correlation is correctly specified in $\mathbf{C}_{s_0}$, then the inversion is able to make larger adjustments to the prior fluxes and achieve a larger uncertainty reduction in these

5   fluxes.

4.3 Relative uncertainty in $\mathbf{C}_{s_0}$

Specification of the uncertainties in the prior flux estimates is one of the most challenging tasks in an atmospheric inversion exercise. There is little consensus on the correct approach to follow, and it is difficult to ensure that the most important sources of uncertainty are accounted for. The degree to which the inversion is constrained by the prior fluxes is inversely related

10   to the specified prior uncertainty. If either the uncertainty in the fossil fuel fluxes or in the NEE fluxes was increased, this led to aggregated flux estimates that were more positive as the inversion was apparently attempting to compensate for the overestimation of the NEE uptake by the CABLE model. When the uncertainties were made smaller, the degree to which the inversion could increase the fluxes was restricted, and the resulting aggregated fluxes were more negative compared with the reference inversion.

15   These sensitivity results illustrate how dependent the uncertainty bounds around the posterior estimates are on the uncertainties specified for the prior fluxes. The inversion relies on the correctness of the uncertainty estimates assigned to the prior fluxes. The posterior uncertainties reflect the reduction in uncertainty achieved by the inversion given that the prior uncertainties are accurate. This motivates for the hierarchical Bayesian approach where a distribution is assigned to the uncertainty estimates. It can be shown that in the absence of observation error, doubling or halving the prior uncertainty in the fluxes results

20   in a respective doubling or halving of the posterior uncertainty (see Supplement Sect. 1.5). Therefore it us unsurprising that if a prior uncertainty is made larger with respect to a reference inversion specification, that the posterior uncertainty of this inversion will be larger than the posterior uncertainty of the reference.

This set of sensitivity tests demonstrated that if we wish to ensure that the uncertainty bounds around the posterior fluxes are within a prespecified margin, say 10% of the aggregated flux estimate, then we have to ensure that prior uncertainty that

25   we begin with is sufficiently small. Assuming no large shifts in the mean estimate, it can be shown that if we wish to obtain an uncertainty estimate that is within 10% of the aggregated flux estimate, and we are able to reduce the uncertainty by 25% through the inversion, then the prior uncertainty estimate would need to be within 13.3% of the prior aggregated flux estimate.

4.4 Homogenised prior information

Applying a spatially homogenised prior for NEE resulted in aggregated prior fluxes with smaller uncertainties, but in aggregated

30   posterior fluxes that were quite different to those of the reference inversion. As the uncertainty was smaller, the degree to which the inversion could adjust these priors was diminished. An alternative sensitivity test could use the mean NEE flux as the prior for all pixels, but the maximum NPP as the uncertainty across all pixels. This would have allowed the inversion to adjust the

fluxes by a much larger degree allowing us to determine how much the inversion wanted to adjust the prior fluxes. Comparing the results to the reference inversion did illustrate that CABLE was most likely over-estimating the amount of CO_2 uptake.

Smoothing the domestic emissions over time had less of an effect on the inversion, with corrections to the prior estimates generally of the same magnitude and in the same direction, and with similar uncertainty reductions.

5 **4.5   Simplified C_c**

Simplifying the C_c had very little impact on the inversion results. Increasing the night-time observation errors caused the aggregated flux to be more negative. Assigning an uncertainty in the night-time modelled concentrations of 10 ppm effectively led to the inversion ignoring most of the information available at night, leaving the posterior night-time fluxes (which are mostly affected by the night-time observations) to be similar to their prior estimates. If the inversion is tending to make large corrections

10 to the daytime fluxes, and is now unable to make large corrections to the night-time fluxes, it implies that the aggregated fluxes will be more in error than if the inversion could be constrained by the observations - provided the constraint is good. The analysis of the misfits in the modelled concentrations from the reference inversion (Nickless et al., 2018) demonstrated that the errors in the day and night-time atmospheric transport modelling were not very different, and therefore it is unlikely that assigning errors as large as 10 ppm to all the night-time observations is necessary. The analysis of the errors in the modelled

15 concentrations between day and night for the reference inversion provided confidence that the approach of increasing the errors only when conditions indicated that errors were more likely led model errors that were similar to those obtained during the day (Nickless et al., 2018).

4.6   Alternative control vectors

The separate weekly inversions obtained similar results to those of the reference inversion. Therefore, if necessary, for example

20 due to computational costs, the separate weekly inversions could have been performed in place of the monthly inversions used in the reference case. In addition to the reduction in computation resources required, this allows additional features of the inversion to be tested more easily.

The large uncertainty reduction achieved by the mean weekly flux inversion is expected as a mean weekly flux estimate over four weeks has four times as many observations to constrain this estimate than if separately weekly fluxes are solved for. The

25 estimates from the inversion solving for a mean weekly flux were consistent with those from the reference inversion, except in the summer months. During these months observations were often missing, and therefore smaller discrepancies may have been observed if data continuity during these periods was similar to the rest of the inversion study period.

An alternative control vector, which could improve on all three of the alternative control vectors used in this study, would be to solve for separate components of fossil fuel and NEE fluxes. For example, if fossil fuel fluxes were split into those fluxes

30 from sectors which change slowly and those which change more quickly, the inversion could solve for a mean weekly flux over the month for the slow fluxes, and for sectors with faster changes, the inversion could solve for individual weekly fluxes. This would allow greater uncertainty reductions for those fluxes for which a mean weekly flux could be solved, which would in turn reduce the overall uncertainty in the aggregated fossil fuel flux. The NEE flux could also potentially be split into a slow and

fast component. The fast component responds to local climate conditions and this component could be tightly constrained by the available climate data. The inversion could solve for the slower component which is much harder to model, and to which we could assign larger uncertainties than we would need to for the fast component. As this is the slower component, we could solve for a mean weekly flux over the month, which would allow greater uncertainty reduction.

4.7 Inversion sensitivity

If we consider the aggregated flux over the full measurement period presented in Table 3, the variability between flux estimates across those inversions which used the reference control vector is 2024 kt CO_2. This is largely driven by the inversions using different prior products, and this uncertainty drops to 487 if these two inversions are removed, and drops further to 393 if the inversions with the transformed prior information are removed. This represents the variability in the aggregated flux estimate across all inversions which used the same prior information products. If we compare this to the uncertainty in the aggregated fluxes, which is approximately 185 kt CO_2, it shows that variability between posterior flux estimates from different inversion frameworks is still very large when compared with the uncertainty we expect around the posterior flux estimates. If the inversions with no error correlation between biospheric fluxes are removed, then the variability between inversions drops to 113 kt CO_2 - now below the expected uncertainty around the posterior flux from a single inversion. All the inversions that we removed from the estimate of variability were those which had a large influence on the error correlations of the NEE fluxes, either because they were specifically manipulated or because they were affected by the choice of prior product. This demonstrates the important role error correlations in the prior fluxes have on the posterior flux estimates obtained from an inversion.

Exceptions are the inversions which changed the prior estimates of the fossil fuel fluxes. These fluxes were not assigned error correlations. Those inversions which altered the prior estimates of the fossil fuel fluxes also had variable aggregated fluxes compared with the reference inversion. This is due to the inversion having limited ability to make large changes to the fossil fuel fluxes. The ensemble of posterior fluxes obtained from inversions with alternative prior fluxes allowed us to determine in which direction the inversion was attempting to adjust these fluxes, and provided us with an interval in which we could deduce the best estimate of the aggregated flux would lie. Changing the control vector also had a large influence on the aggregated flux, but this was largely due to periods with low data completeness.

5 Conclusions

Sensitivity tests have shown that to improve the inversion results for the Cape Town inversion, two important advancements should be made to the inversion framework. Firstly the NEE estimates need to be improved. The results from the reference inversion and from these sensitivity tests clearly indicate that CABLE is generally overestimating the amount of CO_2 uptake in the domain. Where there is more confidence in the estimation of the biogenic fluxes, either from CABLE for an alternative land-atmosphere exchange model, these reduced uncertainties should be incorporated into the prior information, rather than

applying a blanket uncertainty equal to the NPP as done for the reference inversion. For example, over agricultural areas, where the biogenic fluxes may be more reliably modelled, uncertainties may be substantially reduced.

Solving for mean weekly fluxes over a month produced much larger uncertainty reductions. Using an alternative control vector which solves for separate components of the fossil fuel and NEE fluxes that can be split into slow and fast components could take advantage of the larger uncertainty reduction achieved from solving for a mean weekly flux for each month. This could potentially allow the inversion to better distinguish between NEE and fossil fuel fluxes, allowing the inversion to apply corrections to the correct flux, and at the same time obtain aggregated flux estimates with smaller uncertainties than those obtained for the reference inversion. The estimates of the aggregated fluxes was shown to be more reliable in the reference inversion than those for the individual fossil fuel and NEE fluxes (Nickless et al., 2018).

The posterior uncertainties are highly dependent on the prior uncertainties. This was shown across several sensitivity tests, including the inversions which used alternative priors, inversions that used homogenised priors and inversions that adjusted the relative uncertainties of the prior fossil fuel and NEE fluxes. Of more concern is the large impact that the correlation assumed for the NEE fluxes had on the aggregated flux estimates and on the spatial distribution of the posterior fluxes. This has been observed in previous inversions (Lauvaux et al., 2016). Of all the specifications made, the correlation lengths are the most arbitrary, but can redefine the posterior flux estimates. The sensitivity tests suggested that correlations between observation errors were of less importance to the inversion result.

Approaches which attempt to solve for the uncertainties rather than relying on prior estimates may provide better estimates of the true uncertainty bounds around the inversion posterior flux estimates. Ganesan et al. (2014) and Wu et al. (2013) propose an hierarchical Bayesian approach to solve for hyper-parameters of the inversion, including the covariance terms, which could reduce the dependency of inversion results on expert opinion estimates of uncertainty.

These sensitivity analyses did not consider alternative atmospheric transport models. Sensitivity tests on previous city-scale inversions have shown this to be an important source of variation between inversion results (Lauvaux et al., 2016; Staufer et al., 2016). Future work on the Cape Town inversion will consider multiple atmospheric transport models, such as the WRF (Weather Research and Forecasting model coupled with Chemistry) regional climate model.

If enough of these sensitivity tests can be performed, and probability distribution around the posterior fluxes can be determined, which may provide better uncertainty limits around these estimates. The ability of running more inversions in a shorter period of time if a more efficient control vector is chosen would make running many more inversion specifications for such an exercise possible. Assigning probability distributions to these parameters that we test underpins the hierarchical Bayesian approach in Ganesan et al. (2014).

Code and data availability. Data and code related to the Bayesian inversion procedure can be made available upon request

Author contributions. AN installed and maintained all the instrumentation at Robben Island and Hangklip, obtained the measurements and processed these into hourly concentrations, ran and processed the result of the LPDM in Fortran, produced all code and ran the inversion in Python, processed all the inversion results using R Statistical Software, produced all graphics and tables, designed the sensitivity tests, and was responsible for the development of the manuscript which forms part of her PhD. PJR was the main scientific supervisor, oversaw

5   all implementation of the inversion, and provided guidance on the presentation of results. FE provided the CCAM and CABLE data. BE provided guidance on statistical issues. RJS provided guidance on the location of the sites and provided advice on the interpretation of the biogenic fluxes. All authors had the opportunity to comment on the manuscript.

Competing interests. The authors declare that they have no conflict of interest

Acknowledgements. We would like to acknowledge and thank Dr. Casper Labuschagne and Danie van der Spuy of the South African Weather

10   Service for their assistance in maintaining the instruments at Robben Island and Hangklip, and Dr. Casper Labuschagne for his guidance on processing the instantaneous CO_2 concentration data; Martin Steinbacher for providing guidance and schematics on the calibration system used on the Picarro instruments; Robin Poggenpoel and Jacobus Smith of Transnet for allowing us access to the lighthouses; Peter Saaise of Transnet, the Robben Island lighthouse keeper, (and his daughter) for assisting when the instrument was not responding; Marek Uliasz for providing us access to the code for his LPDM model; Thomas Lauvaux for providing guidance on processing the LPDM results and

15   useful discussion on the boundary contribution in the inversion. Use was made of the University of Cape Town ICTS-HPC cluster. Please see http://hpc.uct.ac.za/ for details. We would like to thank Andrew Lewis of the University of Cape Town HPC facility for providing useful advice on improving the efficiency of the Python runs. This research was funded by competitive parliamentary grant funding from the Council of Scientific and Industrial Research awarded to the Global Change Competency Area towards the development of the Variable-resolution Earth System Model (VRESM; Grants EEGC030 and EECM066). Additional funding was obtained from the South African

20   National Research Foundation for the Picarro instrumentation.

References

Archibald, S. A., Kirton, A., van der Merwe, M. R., Scholes, R. J., Williams, C. A., and Hanan, N.: Drivers of inter-annual variability in Net Ecosystem Exchange in a semi-arid savanna ecosystem, South Africa, Biogeosciences, 6, 251-266, doi: 10.5194/bg-6-251-2009, 2009.

Bellassen, V. and Stephan, N.: Accounting for carbon: Monitoring, reporting and verifying emissions in the climate economy, Cambridge University Press, Cambridge, UK, 2015.

Bréon, F. M., Broquet, G., Puygrenier, V., Chevallier, F., Xueref-Remy, I., Ramonet, M., Dieudonné, E., Lopez, M., Schmidt, M., Perrussel, O., and Ciais, P.: An attempt at estimating Paris area CO_2 emissions from atmospheric concentration measurements, Atmos. Chem. Phys., 15, 1707–1724, doi: 10.5194/acp-15-1707-2015, 2015.

Department of Environmental Affairs (South Africa): South African National Terrestrial Carbon Sink Assessment, Department of Environmental Affairs, Pretoria, South Africa, 2015.

Engelbrecht, C. J., Engelbrecht, F. A. and Dyson, L. L.: High-resolution model-projected changes in mid-tropospheric closed-lows and extreme rainfall events over southern Africa. Int. J. Climatol., 33, 173–187, doi: 10/1002/joc.3420, 2013.

Exbrayat, J. -F., Pitman, A. J. Abramowitz, G. and Wang, Y, -P.: Sensitivity of net ecosystem exchange and heterotrophic respiration to parameterization uncertainty, J. Geophys. Res. Atmos., 118, 1640–1651, doi:10.1029/2012JD018122, 2013.

Feng, S., Lauvaux T., Newman, S., Rao, P., Ahmadov, R. Deng, A., Díaz-Isaac, L. I., Duren, R. M., Fischer, M. L., Gerbig, C., Gurney, K. R., Huang, J., Jeong, S., Li, Z., Miller, C. E., O'Keeffe, D., Patarasuk, R., Ser, S. P., Song, Y., Wong, K. W., and Yung, Y. L.: Los Angeles megacity: a high-resolution land–atmosphere modelling system for urban CO_2 emissions, Atmos. Chem. Phys., 16, 9019–9045, doi: 10.5194/acp-16-9019-2016, 2016.

Ganesan, A. L., Rigby, M., Zammit-Mangion, A., Manning, A. J., Prinn, R. G., Fraser, P. J., Harth, C. M., Kim, K. -R., Krummel, P. B., Li, S., Mühle, J., O'Doherty, S. J., Park, S., Salameh, P. K., Steele, L. P., and Weiss, R. F.: Characterization of uncertainties in atmospheric trace gas inversions using hierarchical Bayesian methods, Atmos. Chem. Phys., 14, 3855-3864, doi:10.5194/acp-14-3855-2014, 2014.

Gregor, L. and Monteiro P. M. S.: Is the southern Benguela a significant regional sink of CO2? S. Afr. J. Sci., 109(5/6), Art. #0094, 5 pages, doi: 10.1590/sajs.2013/20120094, 2013.

Gurney, K. R., Razlivanov, I., Song, Y., Zhou, Y., Benes, B., and Abdul–Massih, M.: Quantification of fossil fuel CO_2 emissions on the building/street scale for a large U.S. city, Environ. Sci. Technol., 46, 12194–12202, doi: 10.1021/es3011282, 2012.

Kowalczyk, E. A., Wang, Y. P. and Law, R. M.: CSIRO Atmosphere Biosphere Land Exchange model for use in climate models and as an offline model, CSIRO Marine and Atmospheric Research technical paper xxV ISBN 1 921232 39 0, 2006.

Lauvaux, T., Pannekoucke, O., Sarrat, C., Chevallier, F., Ciais, P., Noilhan, J., and Rayner, P. J.: Structure of the transport uncertainty in mesoscale inversions of CO_2 sources and sinks using ensemble model simulations, Biogeosciences, 6, 1089-1102, doi: 10.5194/bg-6-1089-2009, 2009.

Lauvaux, T., Schuh, A. E., Uliasz, M., Richardson, S., Miles, N., Andrews, A. E., Sweeney, C., Diaz, L. I., Martins, D., Shepson, P. B., and Davis, K. J.: Constraining the CO_2 budget of the corn belt: exploring uncertainties from the assumptions in a mesoscale inverse system, Atmos. Chem. Phys., 12, 337–354, doi: 10.5194/acp-12-337-2012, 2012.

Lauvaux, T., Miles, N. L., Deng, A. Richardson, S. J., Cambaliza, M. O., Davis, K. J., Gaudet, B., Gurney, K. R., Huang, J., O'Keefe, D., Song, Y., Karion, A., Oda, T., Patarasuk, R., Razlivanov, I., Sarmiento, D., Shepson, P., Sweeney, C., Turnbull, J., and Wu, K.: High-resolution atmospheric inversion of urban CO_2 emissions during the dormant season of the Indianapolis Flux Experiment (INFLUX), J. Geophys. Res. Atmos., 121, 5213–5236, doi: 10.1002/2015JD024473, 2016.

McGregor, J. L. and Dix, M. R.: The CSIRO conformal-cubic atmospheric GCM, in: IUTAM Symposium on Advances in Mathematical Modelling of Atmosphere and Ocean Dynamics, Limerick, Ireland, 2–7 July 2000, edited by: Hodnett, P. F., Kluwer, Dordrecht, 197–202, 2001.

Michalak, A. M., Hirsch, A., Bruhwiler, L., Gurney, K. R., Peters, W., and Tans, P. P.: Maximum likelihood estimation of covariance parameters for Bayesian atmospheric trace gas surface flux inversions, J. Geophys. Res., 110, D24107, doi: 10.1029/2005JD005970, 2005.

Moncrieff, G.R., Scheiter,S. Slingsby, J. A. and Higgins, S. I.: Understanding global change impacts on South African biomes using Dynamic Vegetation Models, S. Afr. J. Bot., 101, 16–23, doi: 10.1016/j.sajb.2015.02.004, 2015.

Nassar, R.,Napier-Linton, L., Gurney, K. R., Andres, R. J., Oda, T., Vogel, F. R. and Deng, F.: Improving the temporal and spatial distribution of CO_2 emissions from global fossil fuel emission data sets, J. Geophys. Res. Atmos.,118, 917-–933, doi: 10.1029/2012JD018196, 2013.

Nickless, A., Scholes, R. J. and Filby, E.: Spatial and temporal disaggregation of anthropogenic CO_2 emissions from the City of Cape Town, S. Afr. J. Sci., 111(11/12), Art. $\#2014 - 0387$, 8 pages, doi: 10.17159/sajs.2015/20140387, 2015.

Nickless, A., Ziehn, T., Rayner, P. J., Scholes, R .J., and Engelbrecht, F.: Greenhouse gas network design using backward Lagrangian particle dispersion modelling – Part 2: Sensitivity analyses and South African test case, Atmos. Chem. Phys., 15, 2051–2069, doi: 10.5194/acp-15-2051-2015, 2015.

Nickless, A., Rayner, P. J., Engelbrecht, F., Brunke, E.-G., Erni, B., and Scholes, R. J.: Estimates of CO_2 fluxes over the city of Cape Town, South Africa, through Bayesian inverse modelling, Atmos. Chem. Phys., 18, 4765-4801, doi: 10.5194/acp-18-4765-2018, 2018.

Oda, T. and Maksyutov, S.: A very high-resolution (1 km×1 km) global fossil fuel CO_2 emission inventory derived using a point source database and satellite observations of nighttime lights, Atmos. Chem. Phys., 11, 543-556, doi:10.5194/acp-11-543-2011, 2011.

Oda, T., Lauvaux, T., Lu, D., Rao, P., Miles, N. L., Richardson, S. J. and Gurney, K. R.: On the impact of granularity of space-based urban CO_2 emissions in urban atmospheric inversions: A case study for Indianapolis, IN, Elem Sci Anth, 5, 28, doi: 10.1525/elementa.146, 2017.

Oda, T., Maksyutov, S., and Andres, R. J.: The Open-source Data Inventory for Anthropogenic Carbon dioxide (CO_2), version 2016 (ODIAC2016): A global, monthly fossil-fuel CO_2 gridded emission data product for tracer transport simulations and surface flux inversions, Earth Syst. Sci. Data Discuss., doi: 10.5194/essd-2017-76, in review, 2017.

Roux, B.: Ultra high-resolution climate simulations over the Stellenbosch wine producing region using a variable-resolution model, MSc Thesis, Faculty of Natural and Agricultural Sciences, University of Pretoria, South Africa, 106 pp., 2009.

Scholes, R. J., von Maltitz, G. P., Archibald, S. A., Wessels, K., van Zyl, T., Swanepoel, D., and Steenkamp, K.: National Carbon Sink Assessment for South Africa: First Estimate of Terrestrial Stocks and Fluxes, CSIR Technical Report, Pretoria, South Africa, CSIR/NRE/GC/ER/2013/0056/B, 2013.

Seibert, P. and Frank, A.: Source-receptor matrix calculation with a Lagrangian particle dispersion model in backward mode, Atmos. Chem. Phys., 4, 51–63, doi: 10.5194/acp-4-51-2004, 2004.

Staufer, J., Broquet, G., Bréon, F. -M., Puygrenier, V., Chevallier, F., Xueref-Rémy, I., Dieudonné, E., Lopez, M., Schmidt, M., Ramonet, M., Perrussel, O., Lac, C., Wu, L., and Ciais, P.: The first 1-year-long estimate of the Paris region fossil fuel CO2 emissions based on atmospheric inversion, Atmos. Chem. Phys., 16, 14703–14726, doi: 10.5194/acp-16-14703-2016, 2016.

Tarantola, A.: Inverse Problem Theory and Methods for Model Parameter Estimation, Society for Industrial and Applied Mathematics, Philadelphia, 2005.

Turnbull, J. C., Karion, A., Fischer, M. L., Faloona, I., Guilderson, T., Lehman, S. J., Miller, B. R., Miller, J. B., Montzka, S., Sherwood, T., Saripalli, S., Sweeney, C., and Tans, P. P.: Assessment of fossil fuel carbon dioxide and other anthropogenic trace gas emissions from airborne measurements over Sacramento, California in spring 2009, Atmos. Chem. Phys., 11, 705-721, doi: 10.5194/acp-11-705-2011, 2011.

5   Uliasz, M.: Lagrangian particle modeling in mesoscale applications, in: Environmental Modelling II, Computational Mechanics Publications, Southampton, UK, 71–102, 1994.

Wu, L., Bocquet, M., Chevallier, F., Lauvaux, T., and Davis, K.: Hyperparameter estimation for uncertainty quantification in mesoscale carbon dioxide inversions, Tellus B, 65, 20894, doi: 10.3402/tellusb.v65i0.20894, 2013.

Wu, L., Broquet, G., Ciais, P., Bellassen, V., Vogel, F., Chevallier, F., Xueref-Remy, I., and Wang, Y.: What would dense atmospheric
10   observation networks bring to the quantification of city CO_2 emissions?, Atmos. Chem. Phys., 16, 7743–7771, doi: 10.5194/acp-16-7743-2016, 2016.

Zhang, H., Pak, .B., Wang, Y. P., Zhou, X., Zhang, Y. and Zhang, L.: Evaluating surface water cycles simulated by the Australian community land surface model (CABLE) across different spatial and temporal domains. J. Hydrometeor, 14, 1119–1138, 2013.

Zhang, Y., Gao, Z., Li, D., Li, Y., Zhang, N., Zhao, X., and Chen, J.: On the computation of planetary boundary-layer height using the bulk
15   Richardson number method, Geosci. Model Dev., 7, 2599–2611, doi: 10.5194/gmd-7-2599-2014, 2014.

Ziehn, T., Nickless, A., Rayner, P. J., Law, R. M., Roff, G., and Fraser, P.: Greenhouse gas network design using backward Lagrangian particle dispersion modelling – Part 1: Methodology and Australian test case, Atmos. Phys. Chem., 14, 9363–9378, doi: 10.5194/acp-14-9363-2014, 2014.